Master's thesis

NTNU
Norwegian University of Science and Technology
Faculty of Natural Sciences
Department of Physics

Bjørnulf Brekke

Diagrammatic Monte Carlo based on irreducible vertices for the Hubbard model in the strong-coupling limit

Master's thesis in Physics and Mathematics
Supervisor: Asle Sudbø, IFY
July 2020

NTNU
Norwegian University of
Science and Technology

Bjørnulf Brekke

Diagrammatic Monte Carlo based on irreducible vertices for the Hubbard model in the strong-coupling limit

Master's thesis in Physics and Mathematics
Supervisor: Asle Sudbø, IFY
July 2020

Norwegian University of Science and Technology
Faculty of Natural Sciences
Department of Physics

NTNU
Norwegian University of
Science and Technology

Abstract

We present an introduction to recent diagrammatic methods in the strong-coupling regime, developed by Carlström [1]. The method is specifically applied to the two-dimensional Hubbard model. It serves as an attempt to alleviate the numerical sign problem, characteristic for strongly correlated fermionic systems. The resulting diagrams consist of so-called irreducible vertices that make the system suitable for a systematic diagrammatic Monte Carlo approach. We construct a database for storing the irreducible vertices, making them accessible in the Monte Carlo simulation without any expensive evaluation. Furthermore, we do a partial summation of all irreducible vertices to the lowest order. The partial summation constitutes a single-particle propagator and is an example of a bold propagator method. Based on the irreducible vertices and bold propagators, we suggest a possible implementation for a diagrammatic Monte Carlo approach for the full diagrammatic expansion. To develop a simple method, we use an ergodic set of three update pairs governing the diagram topologies and a set of updates governing internal variables, fulfilling a detailed balance requirement.

Sammendrag

Vi presenterer en introduksjon til nye diagrammatiske metoder i sterk-kobling regimet, utviklet av Carlström [1]. Metoden er brukt spesifikt på den to-dimensjonale Hubbard modellen. Den nyttes som et forsøk på å redusere det numeriske fortegnsproblemet, karakteristisk for sterkt korrelerte fermionsystemer. De resulterende diagrammene består av såkalte irredusible vertexer som gjør systemet passende for en systematisk diagrammatisk Monte Carlo tilnærming. Vi konstruerer en database for å lagre de irredusible vertexene, for å gjøre de tilgjengelig i Monte Carlo simuleringen. Videre gjør vi en delvis summering av alle irredusible vertexer til laveste orden. Den delvise summasjonen utgjør en en-partikkel propagator og er et eksempel på en fet-propagator metode. Basert på irredusible vertexer og fete propagatorer foreslår vi en mulig implementasjon for en diagrammatisk Monte Carlo tilnærming for den fulle diagrammatiske ekspansjonen. For å utvikle en enkel metode bruker vi et ergodisk sett med tre oppdateringspar som styrer diagramtopologiene og et sett med oppdateringer som styrer interne variabler som innfrir et krav om detaljert balanse.

Preface

Acknowledgements

This thesis concludes my five-year Master's degree program in Applied Physics and Mathematics at the Norwegian University of Science and Technology (NTNU). It represents research conducted during the spring semester of 2020, under the guidance of Prof. Asle Sudbø. The project has been exciting to work on and has served as a great introduction to stochastic methods in many-body physics.

I would like to sincerely thank my supervisor Prof. Asle Sudbø, for giving me the opportunity to carry out the project at the Center for Quantum Spintronics. Your encouragement and patience throughout the duration of this thesis have been greatly appreciated. I am also grateful to Even Thingstad, PhD student at the Department of Physics, for countless discussions and invaluable support. Finally, I would like to thank friends and fellow students for a wonderful time at NTNU and Technische Universität München.

Bjørnulf Brekke
Trondheim, Norway
July, 2020

Units

Throughout the thesis, we use natural units. That is, we set the reduced Planck constant $\hbar = 1$ and the Boltzmann constant $k_B = 1$. The lattice constant a is also set to 1.

Contents

Chapter 1

Introduction

1.1 Background and motivation

Feynman diagrams have been an essential tool for theoretical physicists since Richard Feynman introduced them in 1948. The diagrams are useful for describing possible particle processes, including interactions and propagation. The diagrammatic technique is used for a wide range of systems, whereas the nature of the diagrammatic expansion is highly dependent on the system considered [2]. Common for all diagrammatic expansions, is the rapid growth of diagrams and how they represent high dimensional integrals or sums. Monte Carlo methods are ideally suited for evaluating sums and integrals of high dimension, making the combination of the Feynman diagrammatic approach and stochastic computational methods a field of great potential [3].

Interacting many-body systems pose significant difficulties, as the coupling between particles does not allow an independent particle factorization. Although challenging, strongly interacting electron systems give rise to many fascinating phenomena such as magnetic phases and superconducting materials. A wide range of Monte Carlo algorithms has been applied to models for strongly correlated electron systems, such as the Hubbard model [4]. Two examples of such algorithms are determinant quantum Monte Carlo and path integral Monte Carlo methods [5, 6]. Common for most Monte Carlo procedures simulating fermionic systems, is that they encounter the infamous sign problem [7]. The problem is fundamental and in general NP-hard [8]. This means that a solution in polynomial computational time is not expected to exist. Any improvement in the field of computational methods for the Hubbard model is crucial because it is believed to be the theory of high-temperature superconductivity [9].

The severity of the sign problem in conventional quantum Monte Carlo methods scales with the volume of the system, making the thermodynamic limit inaccessible for algorithms such as path integral Monte Carlo. In 1998, Prokof'ev and Svistunov proposed a Monte Carlo method applied directly in the thermodynamic limit, based on sampling Feynman diagrams through a Markov chain Monte Carlo algorithm [10]. The method, called diagrammatic Monte Carlo (diagMC), was implemented for the polaron problem [11], which later has become the arch-example for successful development of diagMC

[10, 12].

Although the diagMC method provides access to observables in the thermodynamic limit, the sign problem is still present. It merely takes a new form and originates from setting a cutoff on an infinite alternating series. A technique for reducing the severity of the sign problem was introduced in 2008. Prokof'ev and Svistunov employed so-called bold propagators in the diagrammatic expansion to increase the radius of convergence [13]. In general, a bold propagator represents a partial summation of diagrams. In this way, the bare propagators can be replaced by propagators accounting for a subset of processes prior to the Monte Carlo simulation. The bold line technique is system dependent, and the scheme generally depends on the type of diagrammatic expansion.

It has the paradoxical feature that a moderate fermionic sign problem improve the convergence properties of the expansion. Unlike bosonic systems, we get cancellation effects from the fermionic sign, effectively reducing the configuration space of the diagMC approach. A developed bold propagator technique is often essential for a diagMC approach dealing with the sign problem.

The bold line technique reduces the configuration space but does not eliminate the factorial growth of diagrams, which is characteristic of any diagrammatic expansion. The factorial growth hinders access to higher-order diagrams. However, the rate of the growth may be reduced through clever expansions and ordering of diagrams. A novel approach was introduced by Carlström [1], where a diagrammatic expansion is performed in both on-site interactions and non-local hopping operators, simultaneously. The resulting contractions are evaluated in so-called irreducible vertices by using recent developments in determinant diagrammatic techniques [14]. An irreducible vertex is here defined as a set of fully connected contractions on a single site. The arising irreducible vertices allow for a systematic diagMC approach where the connectivity of diagrams and the sign of the contributions are considered in a convenient manner. They allow a notably slower factorial growth of diagrams than conventional diagrammatic expansions. This allows higher-order diagrams to be sampled, alleviating the fermionic sign problem.

The main goal of this thesis is to provide a clear and pedagogical introduction to the expansion in irreducible vertices established by Carlström. We include a recursive algorithm for calculating the irreducible vertices and an advantageous form for storing the vertices in a database. Furthermore, we define a bold propagator technique suitable for this specific expansion, including all irreducible vertices to the lowest order. Based on the notion of bold propagators and irreducible vertices, we present a possible implementation using a diagrammatic Monte Carlo approach for the two-dimensional Hubbard model.

1.2 Structure

The Hubbard model, along with a discussion of the Mott-Hubbard transition, is presented in chapter 2. In chapter 3, we develop the theory of a general perturbative expansion and introduce related notions such as time ordering and contractions. The theory is further applied to the two-dimensional Hubbard model, where we perform a perturbative expansion in both the hopping parameter t and the on-site interaction U simultaneously.

Together, chapters 2 and 3 provide a sufficient background for understanding the method of irreducible vertices. This method is thoroughly defined and explained in chapter 4, where we follow Carlström's approach. The main results of the chapter are a recursive approach for calculating vertices and a feasible method for storing vertices in a database. The irreducible vertices are furthermore used as constituents for resulting Feynman diagrams. In chapter 5, we present a specific bold propagator method for the irreducible vertex expansion. Further, we use the irreducible vertices and bold propagators as constituents for a full diagrammatic representation. This includes a discussion of the sign of the contributions following Carlström's use of reference contractions.

In chapter 6, we shift the focus from theoretical considerations to computational methods. A general introduction to Markov chain Monte Carlo is provided, including Markov chains and the Metropolis-Hastings algorithm. Subsequently, we give a thorough introduction to diagrammatic Monte Carlo, as it represents a relatively new set of methods. This includes discussions of the bold line trick, normalization, and convergence properties.

Chapter 7 consists of two parts. The first part considers the process of obtaining numerical values for the bold propagators defined in chapter 5 and serves as an introductory example of diagrammatic Monte Carlo. In addition, we present an alternative semi-analytical approach in chapter 7.2, more suitable for an efficient implementation.

The second part concerns a diagMC implementation for the full diagrammatic expansion based on irreducible vertices. This includes updates changing the diagram topologies and internal variables, including acceptance ratios satisfying the Metropolis choice for a convergent Markov chain Monte Carlo approach. Conclusively, normalization, connectivity, and irreducibility are discussed.

The two parts of chapter 7 present our main contributions in this thesis. It should serve as a pedagogical introduction to the use of diagrammatic Monte Carlo on the expansion in irreducible vertices and as an initial idea for a fully working algorithm. Conclusively, we present a summary of the thesis and mention the remaining steps of the implementation.

Chapter 2

Hubbard Model

2.1 Hamiltonian and Hilbert space

Interacting electron many-body systems as a field of study is exceptionally rich and includes a vast amount of important scientific discoveries. The simplest model accounting for interactions between electrons in a many-body system is the Hubbard model [4]. It considers interacting electrons on a lattice. This deceptively simple model presented in 1963 has been studied for decades, and although simple to write down, it has proven incredibly difficult to solve. That is, the character of its ground state and nature of excited states are still actively researched for dimensions $d > 1$. The Hubbard Hamiltonian consists of a nearest-neighbor hopping term and an on-site interaction

$$H = -t \sum_{\langle i,j \rangle \sigma} (c_{i\sigma} c_{j\sigma}^{\dagger} + c_{i\sigma}^{\dagger} c_{j\sigma}) + \sum_{i} U n_{i\uparrow} n_{i\downarrow} - \mu \left(n_{i\uparrow} + n_{i\downarrow} \right), \tag{2.1.1}$$

where $\langle i, j \rangle$ denotes the nearest neighbor pairs on the square lattice, t denotes the hopping parameter, U the onsite interaction originating from Coulomb interactions and μ the chemical potential. $c_{i\sigma}^{\dagger}$ and $c_{i\sigma}$ denote the fermionic creation and annihilation operators at site i with spin σ. The operators are subject to the anti-commutation relations

$$\{c_{i\sigma}, c_{j\sigma'}^{\dagger}\} = \delta_{ij} \delta_{\sigma\sigma'} \tag{2.1.2a}$$

$$\{c_{i\sigma}, c_{j\sigma'}\} = 0 \tag{2.1.2b}$$

$$\{c_{i\sigma}^{\dagger}, c_{j\sigma'}^{\dagger}\} = 0, \tag{2.1.2c}$$

where $n_{i\sigma} = c_{i\sigma}^{\dagger} c_{i\sigma}$ denote the number operator on site i with spin σ. The fermionic operators (2.1.2) generate the many-particle states

$$|\Psi\rangle \propto \prod_{i\sigma} c_{i\sigma}^{\dagger} |0, 0\rangle \tag{2.1.3}$$

spanning the Hilbert space corresponding to the Hubbard model. $|0, 0\rangle$ denotes the vacuum state. The eigenstates of the number operator $n_{i\sigma}$ on a single site span a local

Hilbert space. Due to the anti-commutation relations (2.1.2), the local Hilbert space is limited to the following four states

$$\{|0,0\rangle, c_{i\downarrow}^{\dagger}|0,0\rangle = |0,1\rangle, c_{i\uparrow}^{\dagger}|0,0\rangle = |1,0\rangle, c_{i\uparrow}^{\dagger}c_{i\downarrow}^{\dagger}|0,0\rangle = |1,1\rangle\}. \tag{2.1.4}$$

The states span an occupational basis and are eigenstates of the on-site interaction $\hat{U}$ and the chemical potential $\hat{\mu}$.

The phase diagram of the system is determined by the relationship between the parameters t, U, μ in addition to the inverse temperature β. Although the behavior is not fully understood, the phase diagram can be obtained in certain limits of the parameters. The system is analytically solvable in both the non-interacting limit $U = 0$ and the atomic limit $t = 0$ and a thorough discussion of both cases is given by Tasaki in Ref. [15].

2.2 Particle-hole symmetry

Considering the chemical potential tuned to half-filling such that $n = 1$, the Hubbard model exhibits a particle-hole symmetry. This symmetry requires a bipartite lattice, such as the conventional square lattice. The particle-hole transformation is explicitly given by the transformation

$$d_{i\sigma}^{\dagger} = (-1)^{i} c_{i\sigma}. \tag{2.2.1}$$

The factor $(-1)^i$ takes the value 1 on one sublattice and (-1) on the other. $d_{i\sigma}^{\dagger}$ denotes a hole-creation operator on site i and spin σ. Creating a hole in this way is analogous to annihilating an electron. The hole operators satisfy fermionic anti-commutation relations, similarly to the electron operators. The particle-hole transformation leaves the kinetic hopping term invariant

$$c_{i\sigma}^{\dagger}c_{j\sigma} \to (-1)^{i+j} d_{i\sigma} d_{j\sigma}^{\dagger} = d_{j\sigma}^{\dagger} d_{i\sigma}. \tag{2.2.2}$$

By performing a trivial shift of the chemical potential, the Hamiltonian can be written in a form such that the particle-hole symmetry is evident in the interaction term. The equivalent form is

$$H = -t \sum_{\langle i,j\rangle\sigma} \left(c_{i\sigma}^{\dagger}c_{j\sigma} + c_{j\sigma}^{\dagger}c_{i\sigma} \right) + U \sum_{i} \left(n_{i\uparrow} - \frac{1}{2} \right) \left(n_{i\downarrow} - \frac{1}{2} \right) - \mu' \sum_{i} \left(n_{i\uparrow} + n_{i\downarrow} \right). \tag{2.2.3}$$

It can now be easily verified that the interaction is invariant under the transformation (2.2.1). This leaves the chemical potential the only part of the Hamiltonian not invariant under the particle-hole transformation. In conclusion, the Hamiltonian is particle-hole symmetric for $\mu' = 0$, which is at half-filling $n = 1$.

2.3 Mott-Hubbard transition

The half-filled Hubbard model with strong interactions $U/t \gg 1$ represents the strongly correlated regime. The strong interactions prohibit doubly occupied sites, and each site must be singly occupied. The wave functions localize due to the energy barrier U, and the system becomes an insulator. This type of insulator is called a Mott insulator and has a different origin compared to conventional band insulators [16].

By reducing the filling fraction, we obtain the dilute limit. In this limit, the interaction U can be considered a weak perturbation, as few electrons are present. The model exhibits characteristics of the weakly interacting electron model and can be considered metallic. Numerous attempts have been made towards understanding the transition between the Mott- and metallic phase [17, 18], but to this day, a solution is not known.

Chapter 3

Finite temperature diagrammatic expansion

The finite temperature behavior of many-body systems includes fascinating properties; among these, temperature-driven phase transitions. Systematic development of quantum field theory for finite temperature is possible, allowing a perturbative treatment of a physical system at finite temperature [19]. In this chapter, we develop the formalism of a general perturbative approach at finite temperature. The formalism is furthermore applied to a diagrammatic expansion in the hopping operator $\hat{t}$ and the interaction $\hat{U}$ for the Hubbard model.

3.1 Finite temperature formalism

The main goal of developing a finite temperature theory is to obtain a systematic method for calculating the thermal expectation values of operators defined in the Heisenberg picture. The Heisenberg picture can be related to the Schrödinger picture, often used in introductory texts to quantum mechanics [20], by incorporating the time evolution into the operators instead of the states. The operators in the Heisenberg picture $\hat{O}_H(t)$ are related to the operators in the Schrödinger picture $\hat{O}_S$ as

$$\hat{O}_H(t) \equiv e^{iHt}\hat{O}_S e^{-iHt}, \tag{3.1.1}$$

where the operators in the Schrödinger picture $\hat{O}_S$ are time-independent by construction and H is the model Hamiltonian. The expectation value in the zero temperature, $T = 0$, case is found by considering the time-independent ground state

$$\langle O(t)\rangle_0 = \langle \Psi_0 | \, \hat{O}_H(t) \, | \Psi_0 \rangle \, , \tag{3.1.2}$$

where $|\Psi_0\rangle$ represents the ground state or a set of ground states for a system with degenerate ground states. In the finite temperature, $T \neq 0$, case it is insufficient to consider the ground state, and a complete set of states spanning the Hilbert space must

be considered. Finite temperature expectation values are evaluated according to the partition function $\mathcal{Z}$ and the density operator $\hat{\rho}$ where

$$\mathcal{Z} = \sum_{\nu} \langle \Psi_\nu | \, e^{-\beta H} \, | \Psi_\nu \rangle \tag{3.1.3}$$

and

$$\hat{\rho} = \frac{e^{-\beta H}}{\mathcal{Z}}. \tag{3.1.4}$$

The expectation value of an operator in the Heisenberg picture at finite temperature, $\langle O(t) \rangle_T$, is then given as

$$\langle O(t) \rangle_T = \mathrm{Tr} \, \langle \Psi | \, \hat{\rho} \hat{O}_H(t) \, | \Psi \rangle \, . \tag{3.1.5}$$

The trace, denoted Tr, is defined as the sum over a complete set of states. Following the Matsubara formalism [19], we introduce a generalized Heisenberg picture in order to treat the time evolution and the Boltzmann weight $e^{-\beta H}$ similarly. This is done by performing a Wick rotation $\tau = it$, where τ is now denoted imaginary time [21]. An operator in the generalized Heisenberg picture can then be related to the Schrödinger picture as

$$\hat{O}_H(\tau) \equiv e^{H\tau} \hat{O}_S e^{-H\tau}. \tag{3.1.6}$$

In the rest of the thesis we will exclusively be concerned with the finite temperature case, hence referring to Eq. (3.1.6) as the Heisenberg picture.

3.2 Correlation function

A central quantity of interest when studying many-body systems is the single-particle correlation function, often called a Green's function. The Green's function quantifies correlations in time and space and provides a basis for evaluating the correlation length of the system. The finite temperature counterpart of the Green's function $G_{\alpha\beta}\left(\mathbf{x}_i, \tau; \mathbf{x}_j, \tau'\right)$ is defined in terms of imaginary time. It is evaluated with respect to the grand canonical ensemble

$$G_{\alpha\beta}\left(\mathbf{x}_i, \tau; \mathbf{x}_j, \tau'\right) \equiv -\mathrm{Tr}\left(\hat{\rho} T_\tau \left[c_{i\alpha}(\tau) c^\dagger_{j\beta}(\tau') \right] \right), \tag{3.2.1}$$

where the fermionic operators are in the Heisenberg picture with spin indices α and β. T_τ is the time ordering operator and is defined as

$$\mathrm{T}_\tau \left[\hat{O}_2(\tau') \hat{O}_1(\tau) \right] = \hat{O}_2(\tau') \hat{O}_1(\tau) \Theta(\tau' - \tau) - \hat{O}_1(\tau) \hat{O}_2(\tau') \Theta(\tau - \tau'), \tag{3.2.2}$$

where Θ denotes the Heaviside step function. The definition of the time ordering operator trivially extends to any finite number of operators. Each commutation of fermionic operators gives rise to a sign due to the anti-commutation relations shown in Eq. (2.1.2). The total number of commutations in order to obtain a time ordered product of operators determines the total sign.

3.3 Perturbation theory

The correlation function can be found by a perturbative treatment of the system. We start out by splitting the Hamiltonian in an unperturbed part H_0 and a perturbation H_1

$$H = H_0 + H_1, \tag{3.3.1}$$

where the $\hat{H}_0$ yields a completely solvable problem. It is now reasonable to treat H_1 through a perturbative expansion if it is proportional to some small parameter α. In order to obtain an expansion in a convenient form, we introduce the interaction picture. In the interaction picture, the time evolution is split between the operators and the states. The states $|\Psi_I(\tau)\rangle$ are defined as

$$|\Psi_I(\tau)\rangle \equiv e^{H_0\tau} |\Psi_S(\tau)\rangle , \tag{3.3.2}$$

where $|\Psi_S(\tau)\rangle$ denotes the state in the familiar Schrödinger picture. The operators in the Heisenberg picture $\hat{O}_H$ and the interaction picture $\hat{O}_I$ are related to the Schrödinger picture as

$$\hat{O}_H(\tau) \equiv e^{H\tau}\hat{O}_S e^{-H\tau} \tag{3.3.3}$$

$$\hat{O}_I(\tau) \equiv e^{H_0\tau}\hat{O}_S e^{-H_0\tau}. \tag{3.3.4}$$

Combined, this gives the following relation between operators in the interaction picture and the Heisenberg picture

$$\hat{O}_H(\tau) = e^{H\tau}e^{-H_0\tau}\hat{O}_I e^{H_0\tau}e^{-H\tau}. \tag{3.3.5}$$

The time dependence of the operators in the Heisenberg picture, may be efficiently related to the interaction picture by introducing the time-evolution operator

$$\hat{U}(\tau_1, \tau_2) \equiv e^{H_0\tau_1}e^{-H(\tau_1-\tau_2)}e^{-H_0\tau_2} \tag{3.3.6}$$

such that

$$\hat{O}_H(\tau) = \hat{U}(0,\tau)\hat{O}_I(\tau)\hat{U}(\tau,0). \tag{3.3.7}$$

The time evolution operator $\hat{U}$ governs the time evolution of the states in the interaction picture. By using $\hat{U}(\tau,\tau')$, we can relate the perturbed eigenstates to the supposedly known unperturbed eigenstates by the Gell-Mann Low theorem [22]. Through a relation between the unperturbed eigenstates and the perturbed eigenstates, we get a perturbative expansion for the thermal expectation value of operators.

The thermal expectation value of a time-ordered product of operators $\hat{A}(\tau'_m)\hat{B}(\tau'_{m-1})...\hat{F}(\tau'_1)$ in the Heisenberg picture, may be expressed as the perturbation series

$$\frac{-\mathrm{Tr}\left(e^{-\beta H_0}\sum_{n=0}^{\infty}\frac{(-1)^n}{n!}\int_0^\beta d\tau_1...\int_0^\beta d\tau_n T_\tau\left[H_1(\tau_1)...H_1(\tau_n)\hat{A}(\tau'_m)\hat{B}(\tau'_{m-1})...\hat{F}(\tau'_1)\right]\right)}{\mathrm{Tr}\left(e^{-\beta H_0}\sum_{n=0}^{\infty}\frac{(-1)^n}{n!}\int_0^\beta d\tau_1...\int_0^\beta d\tau_n T_\tau\left[H_1(\tau_1)...H_1(\tau_n)\right]\right)}, \tag{3.3.8}$$

where the denominator originates from the grand canonical partition function $\mathcal{Z}$. We integrate over all internal times τ_i, while the external times τ_i' remain fixed as they originate from the external operators $\hat{A}(\tau_m')\hat{B}(\tau_{m-1}')...\hat{F}(\tau_1')$. We are interested in this form applied to the single particle Green's function in Eq. (3.2.1)

$$G_{\alpha\beta}(\mathbf{x},\tau;\mathbf{x}',\tau') = \frac{-\mathrm{Tr}\left(e^{-\beta H_0}\sum_{n=0}^{\infty}\frac{(-1)^n}{n!}\int_0^\beta d\tau_1...\int_0^\beta d\tau_n T_\tau\left[H_1(\tau_1)...H_1(\tau_n)c_\alpha(\mathbf{x},\tau)c_\beta^\dagger(\mathbf{x}',\tau')\right]\right)}{\mathrm{Tr}\left(e^{-\beta H_0}\sum_{n=0}^{\infty}\frac{(-1)^n}{n!}\int_0^\beta d\tau_1...\int_0^\beta d\tau_n T_\tau\left[H_1(\tau_1)...H_1(\tau_n)\right]\right)}. \quad (3.3.9)$$

Eq. (3.3.9) represents factorial many terms to each order due to the time-ordering operator T_τ and does not immediately appear manageable. The solution is to use a generalized form of Wick's theorem for finite temperature [23]. It reduces a perturbative expansion as (3.3.8) to an expansion of fully contracted operators [19]. A product of operators is *fully contracted* if each operator in the product is contracted with another operator. A contraction of operators $\hat{A}\hat{B}$, is in the finite temperature formalism defined as

$$\overbrace{\hat{A}\hat{B}} = \left\langle T_\tau\left[\hat{A}\hat{B}\right]\right\rangle_{H_0} = \mathrm{Tr}\left(\hat{\rho}_0 T_\tau\left[\hat{A}\hat{B}\right]\right), \quad (3.3.10)$$

where $\hat{\rho}_0$ is the density operator corresponding to the unperturbed Hamiltonian H_0 such that $\hat{\rho}_0 = \mathcal{Z}^{-1}e^{-\beta H_0}$. For the single particle Green's function, with corresponding fermionic operators, the contractions take the form of bare propagators

$$G^0_{\alpha\beta}(\mathbf{x}_i,\tau;\mathbf{x}_j,\tau') = \left\langle T_\tau\left[\hat{c}_{i\alpha}(\tau)\hat{c}^\dagger_{j\beta}(\tau')\right]\right\rangle_{\hat{H}_0}. \quad (3.3.11)$$

Fully contracted products of operators are the constituents of any diagrammatic analysis. By factorizing sets of disconnected operators, it may be shown that, to all orders, the disconnected contractions cancel exactly to the denominator of the perturbative expansion. A set of contractions is disconnected, if the set can be factored into two disjoint set of contractions. Such a cancellation of the partition function $\mathcal{Z}$ is especially convenient for methods suffering from the fermionic sign problem. In the proceeding we will consider a specific perturbative expansion of the Hubbard Hamiltonian, giving rise to the method of irreducible vertices in diagrammatic Monte Carlo introduced by Carlström [1].

3.4 Expansion in local and non-local parameters

In the separation of the Hamiltonian in Eq. (3.3.1) for the Hubbard model it is customary to choose either the interaction operator $\hat{U}$ or the hopping term $\hat{t}$ as the perturbation H_1 [24, 25]. The choice is usually motivated by wanting a perturbation in a small parameter, to obtain a well-behaved and convergent expansion.

The method of irreducible vertices introduced by Carlström [1] is based on an expansion in both the interaction parameter U and the hopping parameter t, that is $H_1 = \hat{U}+\hat{t}$.

This leaves $H_0 = \hat{\mu}$ both local and bi-linear. In this specific expansion, $\hat{U}$ will serve as a way to connect the operators originating from the hopping operator $\hat{t}$. In the strong coupling limit, where $U \gg 0$, it may seem contradictory to expand in U. However, this will not cause additional bias due to any truncation, as all local interactions are eventually summed to infinite order. Due to the local unperturbed Hamiltonian $H_0 = \hat{\mu}$, all bare propagators must be local as well

$$G^0_{\alpha\beta}(\mathbf{x}_i - \mathbf{x}_j, \tau) = G^0_{\alpha\beta}(\tau)\delta_{ij}\delta_{\alpha\beta}. \tag{3.4.1}$$

The Dirac delta function $\delta_{\alpha\beta}$ originates from the fact that there are no spin-flipping operators in the unperturbed Hamiltonian. Furthermore, this is the case for the full Hubbard Hamiltonian as well. It is instructive to consider an example of a typical term of the expansion for this particular choice of perturbation H_1. We neglect all internal integrations and prefactors for the moment. It can then be written

$$...tc^\dagger_{j\sigma'}c_{l\sigma'}tc^\dagger_{i\sigma}c_{j\sigma}Uc^\dagger_{j\sigma}c_{j\sigma}c^\dagger_{j\sigma'}c_{j\sigma'}tc^\dagger_{i\sigma}c_{j\sigma'}tc^\dagger_{j\sigma'}c_{l\sigma'}... \tag{3.4.2}$$

where it is clear that both the hopping operator $\hat{t}$ and the on-site interaction $\hat{U}$ contribute. From Eq. (3.4.1), it is clear that only contractions between operators on equal sites are non-zero. This vastly reduces the number of contractions to consider. However, for terms with multiple operators on the same site, the number of possible contractions is factorial. The possible contractions on a single site may form connected and disconnected contributions. Due to contributions from both $\hat{U}$ and $\hat{t}$, a single site may host a large number of distinct contractions. This is captured conveniently by introducing the notion of irreducible vertices.

Chapter 4

Method of irreducible vertices

A perturbative expansion in both the non-local hopping operator $\hat{t}$ and the on-site interaction $\hat{U}$ simultaneously, gives a vast number of possible local processes. In order to account for both sign and connectivity of possible contractions, we will, in this section, introduce the notion of irreducible vertices, first presented by Carlström in Ref. [1]. We will first define the notion in terms of connected and disconnected contractions. Further, we introduce a time-trivial operator basis. The basis gives the irreducible vertices a convenient form for storing in a database that is constructed recursively.

4.1 Definition

In order to define the irreducible vertices, we adopt the shorthand notation used by Carlström

$$\Gamma_n \equiv \frac{(-1)^n}{n!} \int_0^\beta d\tau_1 ... d\tau_n T_\tau. \tag{4.1.1}$$

Expanding in both $\hat{t}$ and $\hat{U}$ it is convenient to extend the notation to

$$\Gamma_n \Gamma_m \equiv \frac{(-1)^{n+m}}{n!m!} \int_0^\beta d\tau_1 ... d\tau_{n+m} T_\tau. \tag{4.1.2}$$

The expansion can now be written in a simple form to n'th and m'th order in both the interaction operator $\hat{U}$ and hopping operator $\hat{t}$

$$\sum_n \Gamma_n H_1^n = \sum_{n,m} \Gamma_n \Gamma_m \hat{U}^n \hat{t}^m, \tag{4.1.3}$$

where $H_1 = \hat{U} + \hat{t}$ is the perturbation considered. We now use that $\hat{U} = \sum_i \hat{U}_i$, where i runs over the lattice sites, and expand further to

$$\sum_n \Gamma_n H_1^n = \sum_{m,n_1,n_2...} \Gamma_m \Gamma_{n_1} \Gamma_{n_2} ... \hat{U}_1^{n_1} \hat{U}_2^{n_2} ... \hat{t}^m. \tag{4.1.4}$$

We consider the set of contractions on a single site i and make a distinction between external operators, originating from the non-local operator $\hat{t}$ and local operators originating from the on-site interaction $\hat{U}$. The external operators give rise to external lines connecting the site to diagrammatic elements on other sites.

Figure 4.1 shows two of many ways to contract operators on a single site i. The contractions form one or more pieces connected to external operators. The figure shows two distinct sets of contractions for a site hosting six external operators originating from the hopping operator in Eq. (4.1.4).

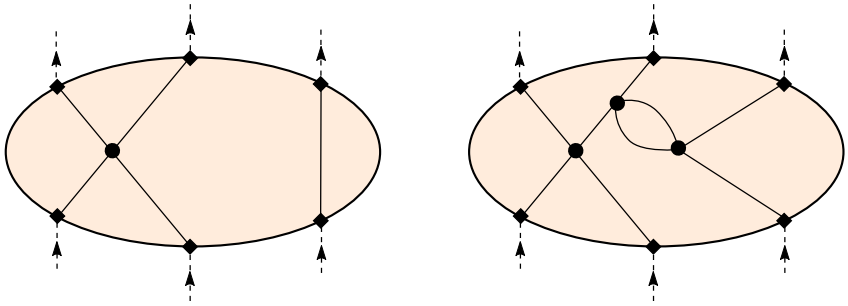

(a) (b)

Figure 4.1: A single site, hosting six external operators visualized as black diamonds at the edge. The on-site interaction U is denoted as black dots. The connectivity in a) shows how the operators form two distinct irreducible vertices, one four-legged vertex, and one two-legged vertex. b) shows all external operators connected forming a single six-legged irreducible vertex.

Proceeding, we consider a finite number of external operators on site i due to $\hat{t}$. We consider the product of operators to be time-ordered, and denote it $\bar{O}$. This means that $\bar{O}$ consists of creation and annihilation operators at imaginary times $\{\tau_1, ...\tau_n\}$. In the following, we do not write the imaginary time dependence explicitly. The product $\bar{O}$ corresponds to a specific order in the hopping operator, but we keep the summation over on-site interactions $\hat{U}$ such that the sum can be taken to infinite order. All possible contractions at site $i$is given by

$$T(\bar{O}) = \pm \sum_n \left\langle \Gamma_n \hat{U}_i^n \bar{O} \right\rangle_\mu . \tag{4.1.5}$$

The sign of this expression is a non-local property, as it depends on how the external operators are contracted with operators on other sites. A thorough discussion of the sign is given in section 5.2.1.

It is necessary to separate the connected set of contractions from the disconnected set of contractions in (4.1.5), in order to develop an efficient diagrammatic approach. This includes separating all sets of contractions that are not connected to any of the external operators $\hat{O}$. The next step is factorizing the internal contractions

$$\sum_n \left\langle \Gamma_n \hat{U}_i^n \bar{O} \right\rangle_\mu = \sum_{n,m} \left\langle \Gamma_n \hat{U}_i^n \bar{O} \right\rangle_{\mu,e} \left\langle \Gamma_m \hat{U}_i^m \right\rangle_\mu . \tag{4.1.6}$$

$\langle ... \rangle_e$ denotes all contractions connected to at least one external operator in the product $\bar{O}$ while the second factor consists of contractions completely disconnected from all external operators. We can rewrite the disconnected contractions

$$\sum_m \langle \Gamma_m U^m \rangle_\mu = \mathrm{Tr}\left(e^{-\beta(\hat{U}+\hat{\mu})} \right). \tag{4.1.7}$$

The set of contractions connected to at least one external leg corresponds to the expectation value of $\bar{O}$ with respect to the local Hamiltonian $H_L = \hat{U} + \hat{\mu}$

$$\sum_n \left\langle \Gamma_n \hat{U}_i^n \bar{O} \right\rangle_{\mu,e} = \langle \bar{O} \rangle_{\hat{\mu}+\hat{U}} . \tag{4.1.8}$$

Due to the locality of the operators such an expectation value is always possible to calculate, by considering the finite Hilbert space shown in Eq. (2.1.4).

Even though all contractions are connected to at least one external operator, this does not imply that all external operators are connected, as shown in figure 4.1 a). We proceed to factorize the subset of contractions into elements where all external operators are connected. In the simplest non-trivial case, we consider a site with four external operators $c^\dagger_{i\sigma}$, $c^\dagger_{i\sigma'}$, $c_{i\sigma}$, and $c_{i\sigma'}$, all originating from non-local hopping processes.

The four operators can be contracted in multiple ways, whereas many of them yield zero. In conclusion, we characterize them by connectivity and write them as a sum,

$$\begin{aligned} \sum_n \left\langle \Gamma_n \hat{U}_i^n c^\dagger_{i\sigma} c_{i\sigma} c^\dagger_{i\sigma'} c_{i\sigma'} \right\rangle_{\mu,e} &= \sum_n \left\langle \Gamma_n \hat{U}_i^n c^\dagger_{i\sigma} c_{i\sigma} c^\dagger_{i\sigma'} c_{i\sigma'} \right\rangle_{\mu,c} \\ &+ \sum_{n,m} \left\langle \Gamma_n \hat{U}_i^n c^\dagger_{i\sigma} c_{i\sigma} \right\rangle_{\mu,c} \left\langle \Gamma_m \hat{U}_i^m c^\dagger_{i\sigma'} c_{i\sigma'} \right\rangle_{\mu,c} \\ &- \sum_{n,m} \left\langle \Gamma_n \hat{U}_i^n c^\dagger_{i\sigma} c_{i\sigma'} \right\rangle_{\mu,c} \left\langle \Gamma_m \hat{U}_i^m c_{i\sigma} c^\dagger_{i\sigma'} \right\rangle_{\mu,c} . \end{aligned} \tag{4.1.9}$$

The subscript $\langle ... \rangle_c$ denotes that all external operators are connected and the minus sign of the third term arises from the commutation of the operators in order to have a time-ordered product of operators. We have successfully decomposed Eq. (4.1.8) into a sum of irreducible vertices, and these vertices will form the basis of the diagrammatic expansion.

For the case of only two external operators, the irreducible vertex takes the simple form of

$$\sum_n \left\langle \Gamma_n \hat{U}_i^n c^\dagger_{i\sigma} c_{i\sigma} \right\rangle_{\mu,c} = \sum_n \left\langle \Gamma_n \hat{U}_i^n c^\dagger_{i\sigma} c_{i\sigma} \right\rangle_{\mu,e} . \tag{4.1.10}$$

It is easily evaluated according to Eq. (4.1.8), as an expectation value. Furthermore, we can generalize the approach to any finite number of external operators. The main idea

is to consider the expectation value as given in Eq. (4.1.8) and to subtract all possible contractions which are reducible. The set of the reducible contractions is captured by

$$\sum_{A\subseteq\bar{O},O_1\in A} \xi_{\bar{O},A} \sum_{n,m} \langle \Gamma^n U^n A\rangle_{\mu,c} \left\langle \Gamma^m U^m \bar{O} \setminus A\right\rangle_{\mu,e}, \tag{4.1.11}$$

where $\xi_{\bar{O},A}$ denotes the fermionic sign originating from the commutations of the operators get a time-ordering

$$T_\tau \bar{O} \to T_\tau A \times T_\tau(\bar{O} \setminus A). \tag{4.1.12}$$

The summation of A is over all proper subsets of $\bar{O}$, such that $\hat{O}_1 \in A$ and all external operators in A is connected. Hence, the expectation value of the operators $\bar{O}$ is now factorized into an irreducible vertex and all possible disconnected contractions. This is done systematically, such that each term consists of a smaller irreducible vertex containing $\hat{O}_1$ and the set of contractions not connected to $\hat{O}_1$.

Furthermore, the scheme can be performed repeatedly by factorizing the second factor of Eq. (4.1.11) into irreducible vertices of fewer external legs. The process terminates in the trivial case shown in Eq. (4.1.10). The recursive relation is now given as

$$\begin{aligned} V[\bar{O}] = &\sum_n \left\langle \Gamma_n \hat{U}_i^n \bar{O}\right\rangle_{\mu,c} = \sum_n \left\langle \Gamma_n \hat{U}_i^n \bar{O}\right\rangle_{\mu,e} \\ &- \sum_{A\subseteq\bar{O},O_1\in A} \xi_{\bar{O},A} \sum_{n,m} \langle \Gamma^n U^n A\rangle_{\mu,c} \left\langle \Gamma^m U^m \bar{O} \setminus A\right\rangle_{\mu,e} \end{aligned} \tag{4.1.13}$$

The recursive procedure is reminiscent of what is done by Rossi in Ref. [14] in a determinant diagrammatic approach. The computational cost is dependent on the number of elements N that can be connected, in this case external operators. The total cost of the recursive algorithm is estimated to $O(N) = 2^N N^3$. The N^3 factor is due the determinants of size N evaluated, while 2^N corresponds to the number of determinants. In Ref. [14], the computational cost is justified by being able to take the thermodynamic limit directly. This is, however, not the motivation in Carlström's method, as the thermodynamic limit is always taken analytically in diagrammatic Monte Carlo.

In contrast to the connected operators in determinant diagrammatic Monte Carlo methods [14], the operators considered in Eq. (4.1.11) are all localized on a single site. This gives the irreducible vertices a convenient form to store in a database, making the computational cost less critical as it is performed before the diagrammatic Monte Carlo simulation. An irreducible vertex represents a large number of ways to connect the external operators, where in each case, all the external operators are connected. The irreducible vertices are used to ensure connectivity of the diagrams in a systematic way, while allowing for a convenient evaluation of the sign of diagrams.

4.2 Analytical form

Eq. (4.1.13) provides both a definition of irreducible vertices and a method for calculating them. Consequently, we can, in principle, calculate irreducible vertices up to arbitrary order. However, calculating the value of an irreducible vertex is computationally expensive, and would not be feasible in an efficient Monte Carlo approach. In this section, we will follow Carlström [1] and develop a convenient form of the irreducible vertices for storing in a database.

In order to handle the time evolution of the external operators $\bar{O}$, we introduce a basis with a trivial time-evolution with respect to the local Hamiltonian $H_L = \hat{U} + \hat{\mu}$. This is done by introducing the operator basis

$$\begin{aligned} c^\dagger_{i\sigma} &= d^\dagger_{i\sigma} + h_{i\sigma} \quad d^\dagger_{i\sigma} = c^\dagger_{i\sigma} n_{i\bar{\sigma}} \quad h_{i\bar{\sigma}} = c^\dagger_{i\sigma}(1 - n_{i\bar{\sigma}}) \\ c_{i\sigma} &= d_{i\sigma} + h^\dagger_{i\sigma} \quad d_{i\sigma} = c_{i\sigma} n_{i\bar{\sigma}} \quad h^\dagger_{i\bar{\sigma}} = c_{i\sigma}(1 - n_{i\bar{\sigma}}). \end{aligned} \tag{4.2.1}$$

The d-operators may be interpreted as creation and annihilation operators for a spin state on a site, given that the complement spin state is occupied. Conversely, the h-operators can be considered creation and annihilation operators, given that the complement spin state is unoccupied. Note how the dagger notation of the h-operators is opposite of that of the c-operators, in reminiscence of the hole-operators defined in section 2.2.

The number of operators in the single-site basis is doubled, rendering a total of eight operators. The advantage of the new basis is that the time-evolution operators can be evaluated with respect to a single state only, hindering the time evolution to mix states. We evaluate the time dependence as

$$\begin{aligned} d^\dagger_{i\sigma}(\tau) &= e^{\tau H_L} d^\dagger_{i\sigma} e^{-\tau H_L} = e^{(U-\mu)\tau} d^\dagger_{i\sigma} \\ h_{i\bar{\sigma}}(\tau) &= e^{\tau H_L} h_{i\sigma} e^{-\tau H_L} = e^{-\mu\tau} h_{i\sigma} \\ d_{i\sigma}(\tau) &= e^{\tau H_L} d_{i\sigma} e^{-\tau H_L} = e^{-(U-\mu)\tau} d_{i\sigma} \\ h^\dagger_{i\bar{\sigma}}(\tau) &= e^{\tau H_L} h^\dagger_{i\sigma} e^{-\tau H_L} = e^{\mu\tau} h^\dagger_{i\sigma}. \end{aligned} \tag{4.2.2}$$

The calculation of the trivial time-evolution is exemplified by considering $d^\dagger_{i\sigma}(\tau)$ applied to its eigenstates. We let $\sigma =\uparrow$ and note that $d^\dagger_{i\sigma}$ annihilates three of the four eigenstates, namely $|1,1\rangle$, $|1,0\rangle$ and $|0,0\rangle$. This leaves $|0,1\rangle$ as the only state with a non-zero contribution, and the Hamiltonian governing the time evolution can be evaluated explicitly

$$\begin{aligned} d^\dagger_{i\sigma}(\tau)\,|0,1\rangle = e^{\tau H_L} d^\dagger_{i\sigma} e^{-\tau H_L}\,|0,1\rangle = e^{\tau H_L} e^{\mu\tau} d^\dagger_{i\sigma}\,|0,1\rangle = \\ e^{(U-2\mu)\tau} e^{\mu\tau}\,|1,1\rangle = e^{(U-\mu)\tau}\,|1,1\rangle \end{aligned} \tag{4.2.3}$$

leaving the time dependence as shown in Eq. (4.2.2). The time-dependent factors can be written as real numbers in the form of exponential functions and then factored out. We can then write the product of external operators in the c-basis with time dependence, as

a sum of products of operators in the time-trivial basis, with a factored time dependence $f(\tau_i)$. The resulting form is

$$\hat{O}_1(\tau_1)...\hat{O}_N(\tau_N) = f_1\left(\{\tau_i\}\right)\hat{o}_{1,1}...\hat{o}_{1,N} + ... + f_M\left(\{\tau_i\}\right)\hat{o}_{M,1}...\hat{o}_{M,N}, \tag{4.2.4}$$

where $\hat{O}_i$ denote operators in the c-basis, while $\hat{o}_{j,l}$ denote the time-trivial part of the operators in the time-trivial basis. The total number of operator products M equals 2^N because for each operator in the c-basis, we obtain two operators in the time-trivial basis. To better understand Eq. (4.2.4), we consider the simple case

$$\hat{O}_1(\tau_1)\hat{O}_2(\tau_2) = c_{i\sigma}(\tau_1)c^\dagger_{i\sigma}(\tau_2). \tag{4.2.5}$$

We transform the operators to the time-trivial basis and factorize the time dependence

$$\begin{aligned} c_{i\sigma}(\tau_1)c^\dagger_{i\sigma}(\tau_2) &= \left(d^\dagger_{i\sigma}(\tau_1) + h_{i\sigma}(\tau_1)\right)\left(d_{i\sigma}(\tau_2) + h^\dagger_{i\sigma}(\tau_2)\right) \\ &= d^\dagger_{i\sigma}(\tau_1)d_{i\sigma}(\tau_2) + d^\dagger_{i\sigma}(\tau_1)h^\dagger_{i\sigma}(\tau_2) + h_{i\sigma}(\tau_1)d_{i\sigma}(\tau_2) + h_{i\sigma}(\tau_1)h^\dagger_{i\sigma}(\tau_2). \end{aligned} \tag{4.2.6}$$

In the present case both cross-terms $d^\dagger_{i\sigma}(\tau_1)h^\dagger_{i\sigma}(\tau_2)$ and $d^\dagger_{i\sigma}(\tau_1)h^\dagger_{i\sigma}(\tau_2)$ vanish. However, in the general case it is not true that all cross-terms evaluate to zero, and a total number of 2^N terms must be evaluated. Eq. (4.2.6) simplifies to

$$e^{(U-\mu)(\tau_2-\tau_1)}d^\dagger_{i\sigma}d_{i\sigma} + e^{\mu(\tau_2-\tau_1)}h_{i\sigma}h^\dagger_{i\sigma}, \tag{4.2.7}$$

giving a simple form for the two-legged vertex. Considering the recursive relation in Eq. (4.1.13), we realize that each term consists of products of expectation values as given in Eq. (4.1.8). In the time trivial basis, this expectation value takes the convenient form

$$\langle o_1(\tau_1)...o_N(\tau_N)\rangle_{\hat{\mu}+\hat{U}} = f(\{\tau_i\})\,\langle o_1...o_N\rangle_{\hat{\mu}+\hat{U}}\,. \tag{4.2.8}$$

The second factor is a time-independent expectation value, namely a real number dependent on the parameters $\hat{U}$, $\hat{\mu}$ and the inverse temperature β. The expectation value is easily evaluated with respect to the local Hamiltonian.

As seen in Eq. (4.1.13), an irreducible vertex consists of a sum of expectation values. Each expectation value is of a distinct subset of the operator product. Every operator subset has a time dependence of the form given in Eq. (4.2.8). However, using the exponent product rule $e^a e^b = e^{a+b}$, the time dependence of each factor adds up to a total time dependence equal for each term in the recursion. This causes a massive simplification, as the time dependence for the connected and disconnected set of contractions are identical. An irreducible vertex may now be stored as a list of time multipliers $[\alpha_1, \alpha_2, ...]$ and a sum of expectation values, adding up to a single expectation value stored as a floating-point number. The simple form of the irreducible vertices makes them suitable for storing in a database.

Table 4.1: Operators in the time-trivial basis and their corresponding numerical representation.

$d_\uparrow^\dagger$	[111]
$d_\downarrow^\dagger$	[110]
$d_\uparrow$	[101]
$d_\downarrow$	[100]
$h_\uparrow^\dagger$	[011]
$h_\downarrow^\dagger$	[010]
$h_\uparrow$	[001]
$h_\downarrow$	[000]

4.3 Construction of database

The irreducible vertices originate from the hopping operator $\hat{t}$ connected by the on-site interaction $\hat{U}$ in the Hubbard model. An irreducible vertex is now defined in terms of the eight operators given in Eq. (4.2.1). This means the number of irreducible vertices scale as 8^N, where N is the number of external operators in the vertex. This scaling effectively limits the maximum number of legs for the irreducible vertices possible to store. However, most of the vertices are zero and do not need to be stored explicitly, similarly to what is done in sparse matrix methods. Note that because the local Hamiltonian conserves the number of particles, N must be an even integer.

Building a database for the irreducible vertices, we may store each operator as a sequence of three boolean values, as this gives $2^3 = 8$ possibilities. More specifically, the first boolean value denotes if it is a d or h type of operator, the second value denotes whether it is a creation operator or an annihilation operator, and the last value determines spin. With the convention that d-type operators, creation operators and spin up correspond to $True$ values, the operators are now represented as shown in Table 4.1.

Now an irreducible vertex may be stored as a string of operators in the form shown in Table 4.1 giving a string of boolean values as

$$d_\uparrow^\dagger d_\uparrow ... h_\downarrow h_\downarrow^\dagger \rightarrow 111101...000010 \tag{4.3.1}$$

For each irreducible vertex represented by a string of boolean values, we store the time multipliers $\{\alpha_i\}$ and the time-independent expectation value. As most products of operators evaluate to zero, we only store finite expectation values. The complete database takes a form similar to the one shown in Table 4.2.

Table 4.2: Irreducible vertices represented as strings of operators with their corresponding time multipliers and a total expectation value.

111101	$[U-\mu,-(U-\mu)]$	$\left\langle d^{\dagger}_{\uparrow} d_{\uparrow} \right\rangle_{\hat{U}+\hat{\mu}}$
011001	$[\mu,-\mu]$	$\left\langle h^{\dagger}_{\uparrow} h_{\uparrow} \right\rangle_{\hat{U}+\hat{\mu}}$
$\vdots$	$\vdots$	$\vdots$
111...101	$[\alpha_1, ..., \alpha_n]$	$\left\langle d^{\dagger}_{\uparrow} ... d_{\uparrow} \right\rangle_{\hat{U}+\hat{\mu}}$

Chapter 5

Expansion based on irreducible vertices

The notion of irreducible vertices gives a convenient way to classify diagrams based on connectivity. The sets of possible contractions can be represented in a diagrammatic manner. A general diagram will then consist of external hopping lines originating from the non-local hopping operator $\hat{t}$ and irreducible vertices. To reduce the space of diagrams, the two-legged irreducible vertices are sorted into *bold* propagator lines. This is a method for limiting the possible diagrams to skeleton diagrams, which is a common approach in diagrammatic Monte Carlo. Skeleton diagrams are often used in quantum field theory when discussing convergence properties of diagrammatic expansions [26]. The use of skeleton diagrams in diagrammatic Monte Carlo, as is the motivation in the present case, is described in section 6.3.

5.1 Definition of bold propagators

The hopping operator $\hat{t}$ between nearest neighboring sites is the only non-local contribution in the Hubbard Hamiltonian. This means that a relatively large diagrammatic space must be considered for any evaluation of non-local Green's functions in position space. This is not feasible for fermionic models suffering from the sign problem, and techniques for reducing the space of diagrams are essential.

We introduce the bold propagator $G_b(\tau, \mathbf{x}; \tau', \mathbf{x}')$ as the sum of a subset of contractions connecting the external operators $c_{i\sigma}(\tau)$ and $c^\dagger_{j\sigma}(\tau')$. In this particular case, the bold propagator represents all two-legged irreducible vertices. Consequently, all two-legged irreducible vertices are accounted for in advance by using bold propagators. It should be noted that a site may host multiple two-legged irreducible vertices.

From a diagrammatic point of view, a bold propagator $G_b(\tau, \mathbf{x}; \tau', \mathbf{x}')$ represents all possible directed paths connecting site i and j, starting at imaginary time τ and ending at imaginary time τ'. An example of directed paths connecting two sites i and j is shown in Figure 5.1. There are, in principle, infinitely many hopping processes connecting two sites. However, each path's contribution is heavily dependent on the length of the path.

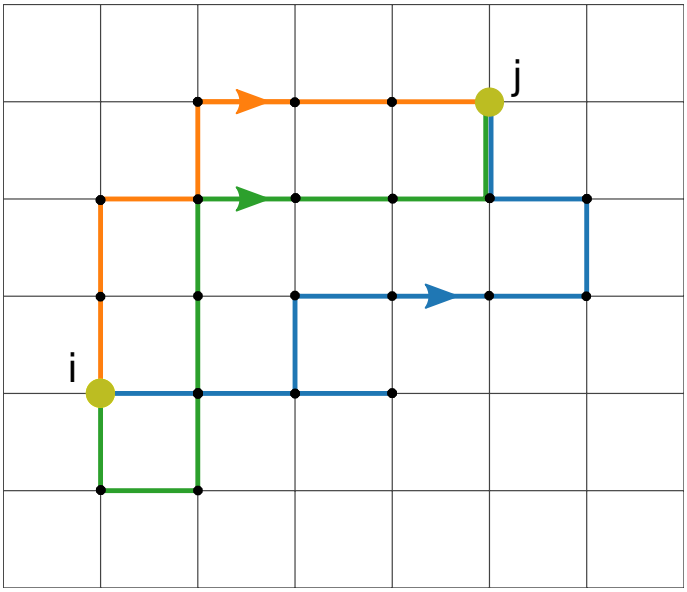

Figure 5.1: Examples of processes contributing to the bold line propagator between site i and site j, where each directed path represents a hopping process. Black dots denote two-legged irreducible vertices, while yellow dots represent more general irreducible vertices. See text for further details.

The length of each path n is determined by the number of hoppings. In this sense, the orange hopping process has a length of 7 hoppings, the green hopping process has length 9, and the blue hopping process has length 11. For each directed path, the contribution is calculated according to

$$G_{\text{path}}(\tau - \tau'; \mathbf{x}_j - \mathbf{x}_i) = t^n \int_0^\beta d\tau_1 ... d\tau_{n-2} \left\langle T_\tau \left(c_i^\dagger(\tau') c_i(\tau_1) \right) \right\rangle_1 ... \left\langle T_\tau \left(c_j^\dagger(\tau_{n-2}) c_j(\tau') \right) \right\rangle_{n-1}, \tag{5.1.1}$$

where t denotes the hopping parameter and T_τ is the time-ordering operator. The fermionic operators $c_i^\dagger(\tau)$ and $c_i(\tau')$, with their respective imaginary times, are the external operators originating from the propagator. The other fermionic operators originate from the hopping operator $\hat{t}$. All fermionic operators are ordered in two-legged irreducible vertices $\left\langle T_\tau \left(\hat{O}_1(\tau) \hat{O}_2(\tau') \right) \right\rangle_{\hat{U}+\hat{\mu}}$.

Feynman rules for bold propagators

We may define the following Feynman rules in order to calculate the bold propagator

1. Construct all distinct and directed paths of length n, connecting site i and site j where each line segment start at a site and end at a nearest neighboring site.

2. For each of the n line segments associate a factor t, denoting the hopping parameter.

3. For each of the $n-1$ irreducible vertices, neglecting the starting point and end-point, associate the thermal expectation value of the vertex and associated time dependence.

4. For each of the $n-2$ internal time variables τ_i, integrate from 0 to β.

The value of a bold propagator, representing all paths connecting two sites i and j, takes the form

$$\begin{aligned} &G_b(\mathbf{x}_i,\tau;\mathbf{x}_j,\tau') = \\ &\sum_n^\infty a_n t^n \int_0^\beta d\tau_1 ... d\tau_{n-2} \left\langle T_\tau \left(c_i^\dagger(\tau') c_i(\tau_1) \right) \right\rangle_1 ... \left\langle T_\tau \left(c_j^\dagger(\tau_{n-2}) c_j(\tau') \right) \right\rangle_{n-1} \end{aligned} \tag{5.1.2}$$

The coefficient a_n denotes the number of paths of length n connecting sites i and j. The exact form of a_n is presented in section 7.2. This leaves the main challenge as to solve the many-dimensional integrals in imaginary time. A product of exponential functions can usually be integrated analytically, however, this is not as simple in the presence of the time-ordering operator.

Properties of the bold propagators

In order to understand the properties of the series in Eq. (5.1.2), we may consider the power series

$$\sum_n^\infty x^n \equiv \sum_n^\infty a_n t^n \int_0^\beta d\tau_1 ... d\tau_{n-2} \{T_\tau[c_i(\tau_1) c_i^\dagger(\tau)]\}_1 ... \{T_\tau[c_j(\tau_{n-2}) c_j^\dagger(\tau')]\}_{n-1}. \tag{5.1.3}$$

The two-legged irreducible vertex can be calculated easily as the thermal expectation value with respect to $\hat{U}+\hat{\mu}$ as shown in Eq. (4.1.8) and Eq. (4.1.10). We assume, without loss of generality, $\sigma = \uparrow$ and let $\tau' > \tau$ such that

$$V[c_{i\uparrow}(\tau') c_{i\uparrow}^\dagger(\tau)] = \mathrm{Tr}\left[e^{-\beta H_L} c_{i\uparrow}(\tau') c_{i\uparrow}^\dagger(\tau) \right]. \tag{5.1.4}$$

To simplify the time dependence, we transform the operators to the time trivial basis in Eq. (4.2.1) and use the trivial time dependence from Eq. (4.2.2) to factorize the time evolution of the operators. This transformation is shown explicitly in Eq. (4.2.6) and evaluating the trace gives

$$\begin{aligned} V[c_{i\uparrow}(\tau') c_{i\uparrow}^\dagger(\tau)] = &\frac{1}{\mathcal{Z}} \Big[e^{(U-\mu)(\tau'-\tau)} \langle 0,1| e^{-\beta H_L} d_{i\sigma} d_{i\sigma}^\dagger |0,1\rangle_{\hat{U}+\hat{\mu}} + \\ &e^{\mu(\tau'-\tau)} \langle 0,0| e^{-\beta H_L} h_{i\sigma} h_{i\sigma}^\dagger |0,0\rangle_{\hat{U}+\hat{\mu}} \Big] \end{aligned} \tag{5.1.5}$$

where the d- and h type operators are defined such that they annihilate all but one state in the occupational number basis in Eq. (2.1.4). Similar arguments for the case $\tau' < \tau$ are used after applying the time-ordering operating, giving the full expression

$$V\left[c_i(\tau')c_i^\dagger(\tau)\right] = \frac{1}{\mathcal{Z}}\Big[\left(e^{-(U+\mu)(\tau'-\tau)}e^{-\mu\beta} + e^{-\mu(\tau'-\tau)}\right)\theta(\tau'-\tau) - \left(e^{-(U+\mu)(\tau'-\tau)}e^{-(U+2\mu)\beta} + e^{-\mu(\tau'-\tau)}e^{-\mu\beta}\right)\theta(\tau-\tau')\Big] \tag{5.1.6}$$

The Green's function is anti-periodic in the time difference $\tau' - \tau$ with a period of β, hence it is sufficient to consider time differences on the interval $[0, \beta]$. Figure 5.2 shows

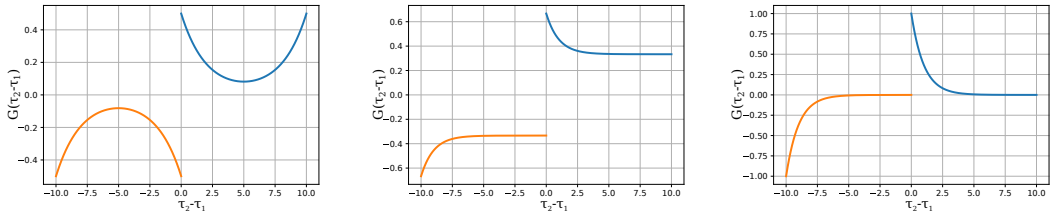

(a) (b) (c)

Figure 5.2: The value of a two-legged irreducible vertex $G(\tau_2 - \tau_1)$ for different values of μ. $\beta = 10$ in units of U and the imaginary time difference $\tau_2 - \tau_1$ may take any value on the domain $[-\beta, \beta]$. a) shows the case for $\mu = \frac{-U}{2}$ where U is the on-site interaction. This is the case of half-filling, and the figure shows a particle-hole symmetry. b) shows the case of $\mu = 0$. c) shows the case of $\mu = U$.

the value of the two-legged irreducible vertices for various values of the chemical potential μ and on-site interaction U for the inverse temperature $\beta = 10$ in units of U. The on-site propagator $G(\tau' - \tau) = \left\langle T_\tau(c_i(\tau')c_i^\dagger(\tau)\right\rangle_{\hat{U}+\mu}$ has a range of $[-1, 1]$.

5.2 Full diagrammatic expansion

With a well-defined notion of irreducible vertices and bold propagators, we may define Feynman rules full propagator $G_{\alpha\beta}(\mathbf{x}_i, \tau; \mathbf{x}_j, \tau')$ associated with the strong-coupling Hubbard model. The diagrams consist of points representing irreducible vertices and dotted lines representing bold hopping lines connecting the vertices. Examples of such diagrams are shown in Figure 5.3.

1. Draw all topologically distinct diagrams with n bold hopping lines following the rules

   (a) Each diagram is connected through irreducible vertices.

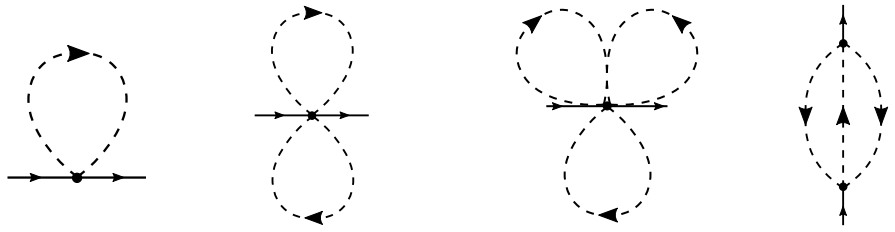

Figure 5.3: Low order diagrams in the expansion based on irreducible vertices. The black dots denote irreducible vertices, with a various numbers of external legs. The dotted lines denote bold hopping lines and the solid lines denote the operators originating from the single-particle Green's function.

   (b) All irreducible vertices have more than two external lines since all simple irreducible vertices are handled in the boldification process. The zeroth-order diagram is an exception, as the external lines are due to the external operators from the single-particle Green's function.

2. For each of the n bold hopping lines associate a factor $G_b(\mathbf{x}', \tau'; \mathbf{x}, \tau)$.

3. For each irreducible vertex, associate the time-dependent value of the irreducible vertex stored in the database.

4. Integrate all out all internal time variables by performing the imaginary time integrals $\int_0^\beta d\tau_i$.

5. For each irreducible vertex, where none of the external operators originate from $G_{\alpha\beta}$, sum over all possible positions $\mathbf{x}$.

6. For each bold hopping line, sum over possible spins $(\uparrow, \downarrow)$.

7. Interpret any bold propagator at equal imaginary time as

$$\lim_{\tau' \to \tau^+} G_b(\mathbf{x}_i, \tau; \mathbf{x}_j, \tau')$$

We denote the number of bold hopping lines in a diagram as the order of the diagram. Some examples of low order diagrams are given in Figure 5.3. Diagram a) is a first-order diagram with a single fourth-order irreducible vertex. Diagram b) and c) are second and third-order diagrams, consisting of six- and eight legged irreducible vertices. Diagram d) differs from the other shown diagrams, as it may contribute to a non-local propagator. This can be seen as it contains bold hopping lines connecting two distinct irreducible vertices.

5.2.1 Sign of diagram

Due to the anti-commutation relations of the fermionic operators, the time-ordering gives rise to the sign of each diagrammatic contribution. In conventional diagrammatics, the sign is determined by the number of fermionic loops. However, in more general models, the sign must be identified through a connection to Wick's theorem [27].

Following Carlström, we introduce a reference contraction, meaning a contraction where the sign is known. Although there are many possible choices for such a contraction, we choose the natural contraction, defined as the case where each operator is contracted with its natural partner. An example of this is

$$...t\overbrace{c_i^\dagger(\tau_1)c_j}(\tau_1)t\overbrace{c_j^\dagger(\tau_2)c_k}(\tau_2)U\overbrace{c_j^\dagger(\tau_3)c_j}(\tau_3)\overbrace{c_j^\dagger(\tau_3)c_j}(\tau_3)... \tag{5.2.1}$$

It is convenient to relate the natural contraction to a reference contraction for the irreducible vertices. A simple way of doing this is to require all external operators contracted with an operator such that all fermionic lines propagate forward in time, are temporally non-intersecting and non-overlapping. An example of such a contraction is

$$\overbrace{c_i^\dagger(\tau_6)c_i}(\tau_5)\overbrace{c_i^\dagger(\tau_4)c_i}(\tau_3)\overbrace{c_i^\dagger(\tau_2)c_i}(\tau_1), \tag{5.2.2}$$

where $\tau_6 > \tau_5 ... > \tau_1$. This particular contraction is shown in Figure 5.4 a) and it can be shown that this contraction carries a positive sign. This is done by relating it to the natural contraction without commuting any of the operators. Such a process conserves the positive sign.

Knowing the reference contraction and its positive sign, we can determine the sign of any given contraction. This is done by relating it through operations and keeping track of any change of sign. It is sufficient to introduce two odd operations. The sign of the contraction is given by the number of performed operations when constructing the reference contraction from the contraction of interest.

We introduce the *commutation* operation which commutes two operators. The operation is odd, due to the anti-commutation relation of fermionic operators. For the reference contraction shown in Eq. (5.2.2), the application of the commutation operator performs the transition from Figure 5.4 a) to b). The second basic update required is the *swap* operator. It swaps the connectivity of external operators. This operation may connect distinct irreducible vertices and hence construct a connected diagram contributing to the observable of interest. The swapping of operators in the reference contraction in Eq. (5.2.2), is shown in Figure 5.4 a) to c).

The reference contraction of a six-legged irreducible vertex and examples of the commutation and swap operations are shown in Figure 5.4 a) to d). a) shows the reference contraction where all external lines are connected, non-intersecting, and propagate forward in imaginary time. The irreducible vertices, a) and b) are connected by a *commute* update. Similarly, one can go from a) to c) by applying the *swap* update. Consequently, both b) and c) carry a negative sign. Further, d) is connected to b) by either a *commute* or *swap* update, while c) and d) are connected by a commutation giving a positive sign for d).

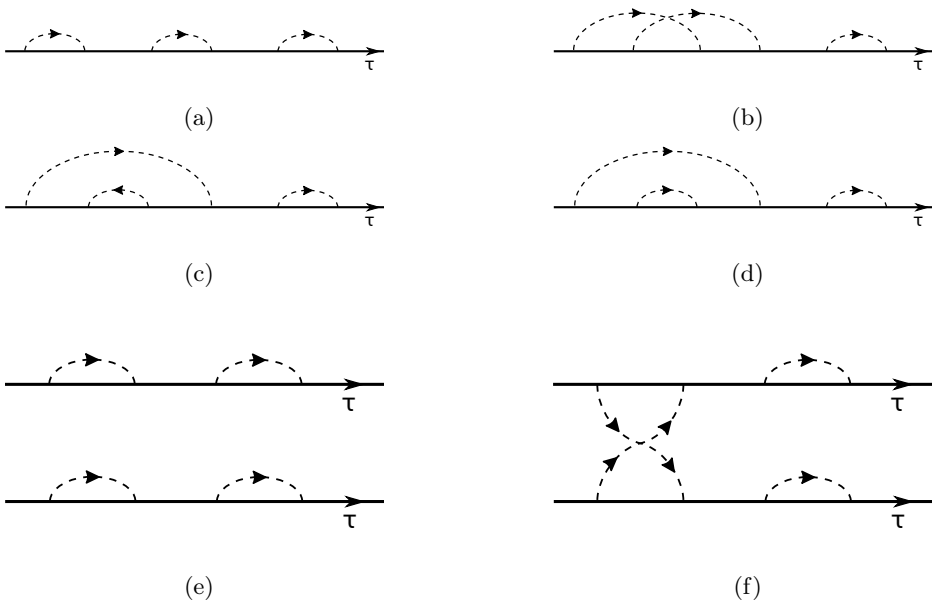

Figure 5.4: Contractions on irreducible vertices. The irreducible vertices are related by the odd operations *commute* and *swap* and can be used to determine the sign of the contributions. See text for details.

Diagrams consisting of more than one irreducible vertices, can give rise to non-local contributions. An example of such a contribution consisting of two four-legged irreducible vertices is shown in Figure 5.4 e). The diagram is disconnected but still carries a positive sign. It is related to f) by the *swap* update, rendering the sign of f) negative.

The case of two-legged vertices, constituting the bold propagator, is particularly simple. As in the general case, the reference contraction is given as only forward propagating hopping lines, as shown in Figure 5.5. The sign of any bold hopping line can now be found as a two-step process. For each irreducible vertex, we can *commute* the external operators, such that a negative sign arises for each commutation needed. Secondly, in order to connect the irreducible vertices, the connectivity of lines are swapped. The sign obtained from the number of *swap* updates is given by the number of irreducible vertices. In total, the sign is given as $(-1)^{c+s}$ where c denotes the number of commutations and s denotes the number of hoppings.

It is, in general, computationally expensive to find the sign of a diagram, as it is a non-local property. In a diagrammatic Monte Carlo approach, the solution is to, for each diagrammatic update, keep track of the parity of the update. Updates constituting a diagrammatic Monte Carlo algorithm are in general more complex than the *commute* and *swap* update. However, these updates can be used to determine the parity of the update and hence keep track of the sign of the total contribution.

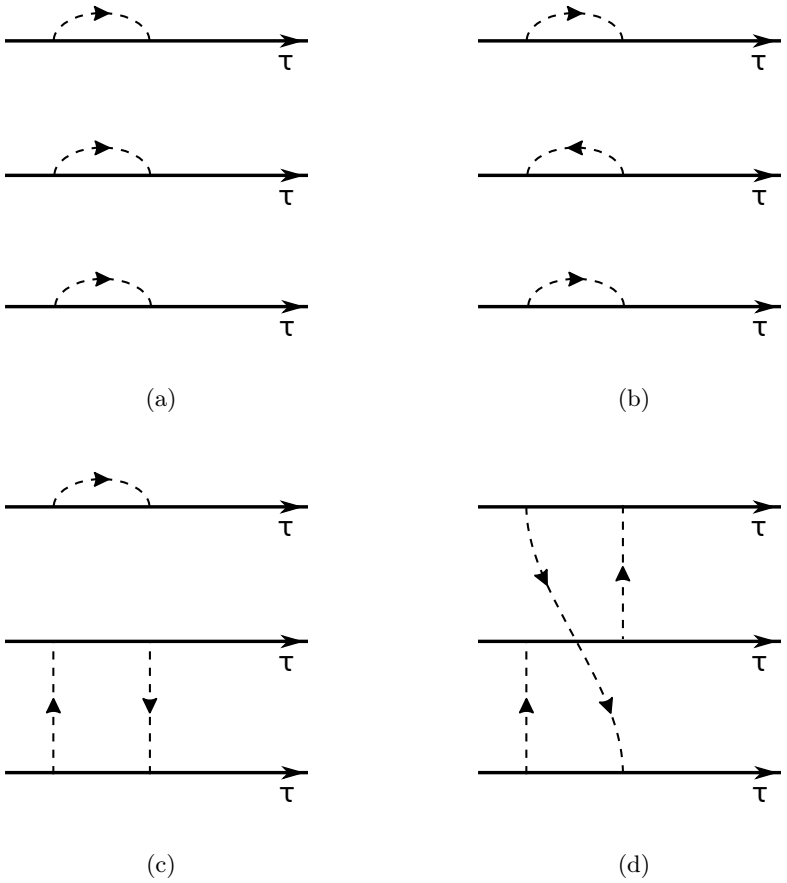

Figure 5.5: The figures a) to d) show the odd operators *commute* and *swap* applied in order to construct a set of three connected two-legged irreducible vertices. By connecting the irreducible vertices by odd operators, we obtain the sign of the contribution.

Chapter 6

Markov chain Monte Carlo

This section will include a general introduction to Markov chain Monte Carlo, a numerical method well-suited for calculating physical quantities in many-body systems. The main idea of any Markov chain Monte Carlo method is to do a stochastic sampling of a stationary distribution. In 1998, Prokof'ev and Svistunov used this method to sample diagrammatic contributions to physical observables, introducing the diagrammatic Monte Carlo (diagMC) method [10]. This method and its developments will be the main topic of this section.

6.1 Markov Chains, ergodicity and balance equations

A Markov chain is a stochastic procedure giving rise to a sequence of states, such that the probability distribution for x_{j+1} given that the system is in state x_j is independent of the state x_{j-1}. That is, given an initial state x_0 the process generates a sequence of states $x_0, x_1, x_2, x_3....$ The sequence is stochastic, and we denote the probability of generating a state x' given a state x as the transition probability $P(x' \to x)$. The set of possible states $\{x_i\}$ is called the configuration space $\mathcal{S}$. For complex systems with a configuration space too large to sample completely, Markov Chains can be used to construct a stationary distribution [28].

In Markov chain Monte Carlo each state $x \in \mathcal{S}$ needs to be sampled according to its importance, or weight $\pi(x)$. In order for the Markov chain to visit the states x_i according to this underlying stationary distribution, two properties are required, namely the ergodic property and global balance.

A Markov Chain is ergodic if, for any initial state x_i, any state in the configuration state can be reached in a finite number of steps through transitions with a finite transition probability. This is required, as a non-ergodic Markov process would assign a false zero probability to states with a finite weight.

In order to obtain the stationary distribution, the weight of each state must be conserved. This is ensured by requiring that for each state x

$$\sum_{x'} \pi(x)P(x \to x') = \sum_{x'} \pi(x')P(x' \to x), \tag{6.1.1}$$

where $\pi(x)$ denotes the weight of the state x and the sum runs over all states in the configuration space. The requirement is called global balance, and ensures that the resulting distribution is stationary. Although ergodicity and global balance are sufficient conditions for the process to converge to the underlying stationary distribution, the requirements do not guarantee an efficient algorithm. For an efficient Markov process the choice of updates and transition probabilities is essential.

Algorithms ensuring global balance may be very efficient [29, 30]. In practice, often, an even stricter condition is used, called detailed balance. Although more restrictive, it is often easier to implement and to enforce. Detailed balance implies global balance, and requires the following to hold for each possible transition

$$\pi(x)P(x \to x') = \pi(x')P(x' \to x). \tag{6.1.2}$$

In practice, $\pi(x)$ is proportional to the underlying physical distribution, while $P(x \to x')$ is determined by the specific algorithm used. An ergodic Markov chain with detailed balance is shown in figure 6.1.

The states in the Markov chain are typically autocorrelated and does not provide an independent equilibrium distribution. In order to reduce the autocorrelation between measurements, we typically only measure each N_τ'th state. N_τ is an integer chosen, preferably of the order of autocorrelation time.

6.2 Metropolis-Hastings

The Metropolis-Hastings algorithm [31] is a Markov chain Monte Carlo method suitable when the relative weight of each state x is known. That is, a distribution function $\Pi(x)$ is known such that $P(x) = \frac{1}{\mathcal{Z}}\Pi(x)$ is a normalised distribution. $\mathcal{Z}$ is often extremely difficult to calculate; however, for the Metropolis-Hastings algorithm, it is sufficient to know the relative weights $\pi(x)$.

The method consists of a number of steps. From an arbitrary state x, an update $x \to x'$ is proposed. The update is accepted with a probability $W_a(x \to x')$ such that the detailed balance requirement is fulfilled. In order to determine the acceptance probability W_a, we decompose the transition probability $P(x \to x')$ into an proposal probability $Q(x \to x')$ and the acceptance probability $W_a(x \to x')$ such that

$$P(x \to x') = Q(x \to x')W_a(x \to x') \tag{6.2.1}$$

The proposal probability $Q(x \to x')$ is, in general, dependent on the number of possible updates and the nature of the configuration space $\mathcal{S}$. In more sophisticated algorithms, importance sampling can be used to obtain acceptance probabilities $W_a(x \to x')$ close to unity. This will, in general, reduce the auto-correlation time.

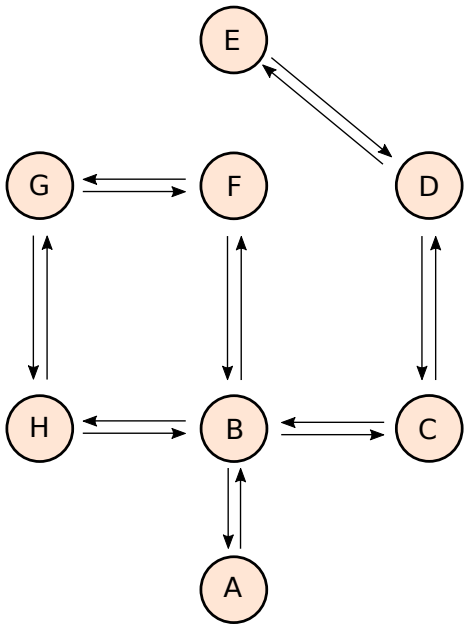

Figure 6.1: An ergodic Markov chain with transitions according to detailed balance. A pair of arrows denote a set of reverse updates with probabilities related through detailed balance requirement. Each letter corresponds to a state, and is sampled according to its weight π.

There is in general some freedom of choice determining the acceptance probability, fulfilling detailed balance. One of the most common approaches is the Metropolis choice

$$W_a(x \to x') = \min\left(1, \frac{\pi(x')Q(x' \to x)}{\pi(x)Q(x \to x')}\right). \tag{6.2.2}$$

Using the Metropolis choice, a Markov chain Monte Carlo algorithm can be broken down into the following steps

1. Initialize the system by choosing an arbitrary state x_0 and setting the Monte Carlo time $t = 0$.
2. Traverse the configuration space $\mathcal{S}$ by iteration
   (a) Generate a new state x' from the proposal distribution $Q(x \to x')$.
   (b) Calculate the acceptance probability $W_a(x \to x')$ through the Metropolis choice criterion.
   (c) Either accept or reject the update by generating a (pseudo-) random number u from a uniform distribution $[0, 1]$.

- If $u < W_a$, accept the update. Let $x_{t+1} = x'$. Increment the Monte Carlo time t by setting $t = t + 1$.
- If $u > W_a$, reject the update. Let $x_{t+1} = x$. Increment the Monte Carlo time t by setting $t = t + 1$.

3. Thermalize the system by performing the iterative scheme (2) until $t = t_{\text{thermal}}$ thermal, where t_{thermal} corresponds to the longest possible autocorrelation time. This ensures the sampling process is independent of the arbitrary initialization.

4. Continue the iterative scheme. For every N_τ'th iteration, perform a measurement.

6.3 Diagrammatic Monte Carlo

In this section, we introduce the ideas behind diagrammatic Monte Carlo. The general concepts will then further be used to develop an efficient algorithmic to evaluate the diagrammatic expansion introduced in section 5.2.

Diagrammatic expansion

The main goal of any diagrammatic approach is to estimate a quantity $Q(y)$ by evaluating a series of Feynman diagrams. This is a well-established approach in quantum field theory [32]. The diagrammatic expansion can be evaluated as an infinite sum, where each term consists of a multidimensional integral over internal variables. Following the introduction to diagrammatic Monte Carlo by Van Houcke et al. [33], we may write a general diagrammatic expansion as

$$Q(y) = \sum_{m=0}^{\infty} \sum_{\xi_m} \int \mathcal{D}(\xi_m, y, x_1, ..., x_m)\, \mathrm{d}x_1 ... \,\mathrm{d}x_m, \tag{6.3.1}$$

where y corresponds to a set of external variables determining the quantity Q, m is the order of the diagram, whereas ξ_m distinguishes the various diagrams of order m. For each diagram, $\mathcal{D}(\xi_m, y, x_1 ... x_m)$ denotes its integrand, with the internal variables $\{x_i\}$. Note that for any discrete internal variable, the integral takes the form of a sum. Relevant examples of this are lattice positions and internal spin variables.

The idea of using a Markov chain Monte Carlo approach to evaluate a diagrammatic expansion of the type in Eq. (6.3.1) was introduced by Prokof'ev and Svistunov in 1998. They provided an approach for the polaron problem [10]. The configuration space $\mathcal{S}$ associated with the method generally consists of all possible diagrams up to fixed order m_{max}, with their respective internal variable configuration. In this way, the method performs both the sum over all diagrams and the internal integrals, simultaneously.

For a fermionic system, the expansion in Eq. (6.3.1) consists of both positive and negative terms $\mathcal{D}$. In order to deal with this, the weight of each state is given by the absolute value $|\mathcal{D}|$ and sampled accordingly. The sign of the contribution $s_{\mathcal{D}} = \pm 1$ is taken into account as the contribution from a given measurement. The number of diagrams scales

factorial with the order m, while the value of each diagram decreases exponentially with the order, due to some small expansion parameter g. As the factorial growth is larger than the exponential decay for large m, this leaves the total weight of the configuration space $\mathcal{S}$ unbounded. For the Markov process to converge to a stationary distribution, a cutoff in the order m is needed. This can be done with a soft cutoff, adjusting the associated weight of high-order terms, or a hard cutoff at $m_{\max}$. To extrapolate the answer to the $m \to \infty$ limit, one may apply resummation techniques. Figure 6.2 shows a typical configuration space in diagMC, where the dimension of the integral represented by diagrams, increases with their order, and the number of diagrams to a given order m is typically factorial large. A diagMC approach samples both the distinct diagram topologies and the domain of internal variables.

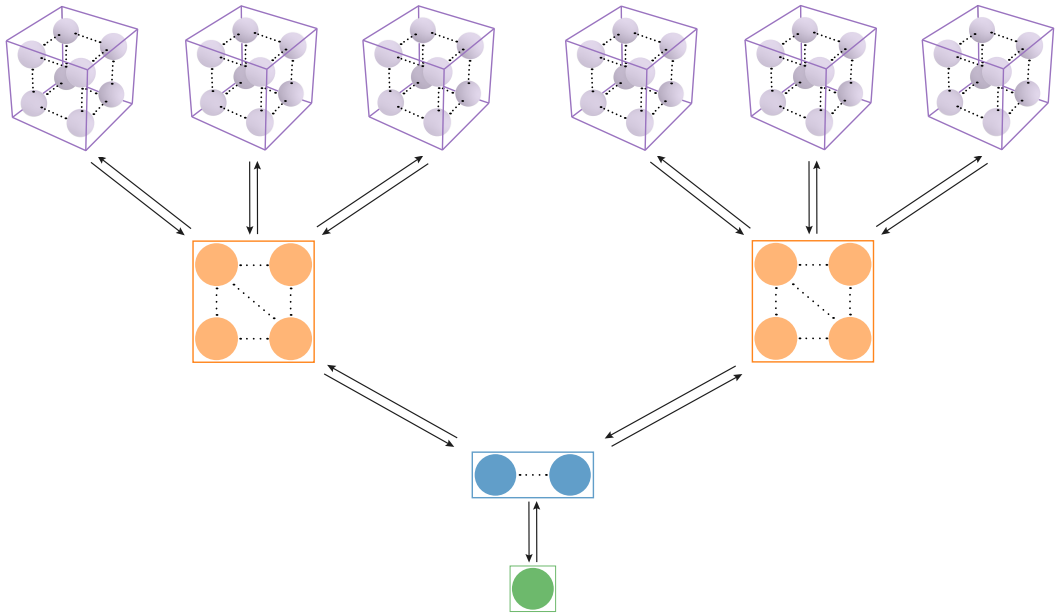

Figure 6.2: A typical configuration space in a diagrammatic Monte Carlo algorithm. Each generalized box represents a diagram, while each generalized sphere represents a set of internal variables. The levels, separated by distinct colors, represent the order of the diagrams, whereas the upper-level boxes denote diagrams of a higher order. The dimension of the internal integrals scales linearly with the order of the diagram, while the number of diagrams of a given order scales factorial.

Sign problem

The rapid sign alternation of the expansion in Eq. (6.3.1) causes massive cancellation between terms of a given order m. The cancellation is the manifestation of the fermionic sign problem and generally hinders sensible results for quantum Monte Carlo methods. In other quantum Monte Carlo methods such as path integral Monte Carlo and auxiliary field Monte Carlo [34, 35], the sign problem scales exponentially with the system size. This makes the thermodynamic limit inaccessible. In contrast, diagrammatic Monte Carlo works directly in the thermodynamic limit. This is one of the big advantages of the method.

The sign problem is still present and merely takes a different form. The sign problem causes an exponential scaling of computation time with the maximum order m_{max}. This makes it difficult to extrapolate the quantity $Q(y)$ to the $m \to \infty$ limit. Many tricks can be employed to alleviate the sign problem in diagrammatic Monte Carlo.

The method can be naturally combined with an analytical evaluation of diagrams, reducing the sampled configuration space. Any analytically evaluated term should be left out of the Markov chain, and the contribution is instead added subsequently. This is especially relevant for low order diagrams.

Bold propagators

The method of bold propagators is an essential technique for any diagrammatic Monte Carlo approach for fermionic systems [13]. The main goal of the method is to reduce the number of diagrams in the configuration space. This is essential, as the fermionic sign problem scales exponentially with the number of diagrams, and any reduction of the diagrammatic space alleviates the problem. The method of bold propagators is a family of methods where the bare propagator $G_0(\tau, \mathbf{x}; \tau', \mathbf{x}')$ is replaced with a bold propagator $G_b(\tau, \mathbf{x}; \tau', \mathbf{x}')$. The bold propagator accounts for a number of processes not included in the bare propagator, reducing the sampling space. The arch-example of a bold propagator approach is the Dyson's equation [27].

An extension of the bold propagator method is, to sum up, certain contributions to the propagator prior to the diagMC algorithm. This approach is highly dependent on the system considered, and the boldification scheme may be implemented to various degrees. Common for all systems is the cancellation effect, which is accounted for in advance. For the polaron problem, the process is performed by solving the Dyson equation for certain diagrammatic elements self-consistently.

Convergence properties of diagrammatic expansion

The convergence properties is an important issue for any diagrammatic expansion. The expansion in Eq. (6.3.1) can be written as a power series

$$\sum_{n}^{\infty} a_n g^n \tag{6.3.2}$$

where n denotes the order of a set of diagrams, g is the expansion parameter and a_n is some coefficient. For such a series, the radius of convergence R is defined as

$$R \equiv \frac{1}{\limsup_{n\to\infty} |a_n|^{\frac{1}{n}}} \tag{6.3.3}$$

where $\limsup_{n\to\infty}$ denotes the upper bound of the possibly oscillating nature of a_n as $n \to \infty$. For $|g| > R$ the series diverges, as the general term $a_n g^n$ does not go to zero as $n \to \infty$. If $|g| < R$ the series converges absolutely

$$\sum_{n=0}^{\infty} |a_n g^n| < \infty \tag{6.3.4}$$

In the case of a diagrammatic expansion, the form of a_n is non-trivial. It is a finite sum over diagrams, such that

$$a_n = \sum_D b_D \tag{6.3.5}$$

where D is a diagram, and b_D denotes the value of the diagram. In order to find an expression of a_n, one would in principle have to count the number of diagrams with order n, and calculate them. The number of diagrams to a given order depends on the expansion in question, but typically scales factorial with n. In a sign alternating series cancellation effects occur and we may have

$$\left| \sum_D b_D \right| \ll \sum_D |b_D| \tag{6.3.6}$$

as b_D takes both positive and negative values.

For bosonic theories like Euclidean ϕ^4-theory [32], all terms are positive, resulting in $R = 0$. In contrast, for fermionic theories, a finite convergence radius is possible. The convergence properties can, however, only be checked a posteriori [36]. The possibility of convergent diagrammatic series is sometimes called a sign blessing [37]. It should be noted that divergent diagrammatic series are still often of great interest, as they tend to diverge asymptotically.

Updates

The stochastic sampling of $Q(y)$ in diagrammatic Monte Carlo generally consists of two parts. The first part consists of updates transitioning between different diagrams and is arguably the most interesting part. In mathematical terms, this means updates changing the structure of the kernel $\mathcal{D}(\xi_m, y, x_1, ..., x_m)$ in Eq. (6.3.1). There are numerous types of possible schemes, and the approach is highly dependent on the expansion in question. A method proven successful is the worm-algorithm introduced by Boninsegni et al. [38]. The method used for the expansion in irreducible vertices is thoroughly discussed in section 7.3.

The second part involves updates changing the internal or external variables $(y, x_1, ..., x_m)$ for a given diagram, without changing the structure of the kernel $\mathcal{D}$ itself. The procedure is similar to the case of sampling multidimensional integrals and sums over the set of internal variables $\{x_i\}$.

Normalization

The samples measured through the Monte Carlo scheme mimics the underlying distribution governing the physical system, up to a constant factor C, when the number of measurements $N \to \infty$. The constant C is directly proportional to the computational time and does not carry physical significance. To normalize the sampled distribution, we denote a set of states $\{x_i\}$ as the normalization bin. The states forming the normalization bin may be physical or unphysical. If they are physical they contribute to the sampled statistics as well. After a completed sampling process, the full distribution is normalized, such that the states in the normalization bin take their proper, known value. For an unphysical state, the weight is arbitrary but should be both sampled and normalized according to its chosen weight. A conventional method in diagMC is to introduce an unphysical zeroth-order diagram and normalize with respect to it.

Symmetries of the real space and imaginary time scheme

Diagrammatic Monte Carlo schemes can be performed in real space or momentum space and with imaginary time or in Matsubara frequency formalism. Imaginary time is often preferred, in order to avoid having to deal with poles [33], while both momentum space and real space algorithms can be efficient.

While boldification methods deal with the reduction of the diagrammatic states, there are also numerous ways to reduce the space of internal variables using the symmetries of the model Hamiltonian. This section introduces the possible symmetries for the Hubbard model in real space and imaginary time on a two-dimensional lattice. The imaginary time τ is discretized into N time steps of length $\Delta\tau$, in order to have states with finite weight π. As the Hamiltonian (2.1.1) has temporal and spatial translational invariance, the correlation function is translational invariant as well,

$$G(\tau, \mathbf{x}; \tau', \mathbf{x}') = G(\tau - \tau'; \mathbf{x} - \mathbf{x}'). \tag{6.3.7}$$

This reduces the space of external variables sampled considerably.

Due to the properties of the trace function Tr, the Green's function for fermions must be anti-periodic in the imaginary time τ [27]. Hence, it is sufficient to restrict the external difference $\tau - \tau'$ to the interval $[0, \beta]$. The domain of all internal times is limited to the compact interval $[0, \beta]$, leaving all temporal integrals convergent.

A further restriction can be made by utilizing the spatial symmetries of the square lattice. The Hamiltonian is invariant under inversions about the x-axis and y-axis, namely the transformation $x \to -x$ and $y \to -y$. A third symmetry is given by exchanging x and y. In conclusion, we can divide the two dimensional lattice into $2^3 = 8$ equivalent

sections and map all points to the first half-quadrant. A natural choice, is to map all points to the section $\{x > 0, y > 0, x > y\}$ as shown in figure 6.3.

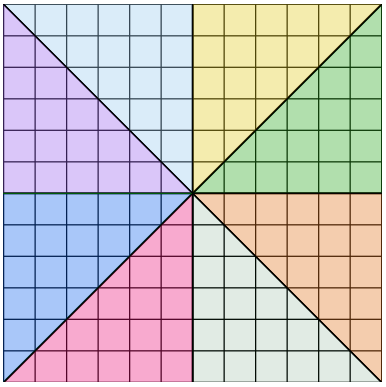

Figure 6.3: The eight equivalent sections under the three symmetries $x \to -x$, $y \to -y$ and $x \to y, y \to x$.

Chapter 7

Implementation of diagrammatic Monte Carlo

In the following section, we will introduce a diagrammatic Monte Carlo (diagMC) scheme based on the principles presented in section 7.3. In the first part, a diagMC scheme for the boldification of hopping lines is introduced. This is needed both for the full implementation of the diagrammatic approach, in addition to serving as an example of a diagMC algorithm. Furthermore, we introduce a diagMC scheme for the full expansion in Eq. (4.1.4), represented with diagrams in real space and imaginary time. In this algorithm, the use of irreducible vertices and bold hopping lines are combined.

7.1 Diagrammatic Monte Carlo as bold propagator scheme

The goal of a boldification process is to evaluate the power series defined in Eq. (6.3.2) partially. In this section we will develop a scheme for calculating a bold propagator according to our definition in section 5.1. The bold propagator will then include all two-legged irreducible vertices. The partial summation of the power series will hence include all paths connecting two points in space $\mathbf{r}$ and $\mathbf{r}'$ at different times τ and τ'.

The main idea of the boldification process is to consider all contributions from two-legged irreducible vertices. The implementation of the bold propagator scheme is done in an object-oriented manner. Each path is represented as a doubly-linked list of irreducible vertices. The information stored in such a vertex consists of time variables τ_1 and τ_2 for the fermionic creation and annihilation operators, respectively, a position (x, y) on the two-dimensional square lattice and pointers to the previous and next irreducible vertex.

The weight of a path is found from considering the contractions and depends exclusively on the length and time configuration of the path, given the input parameters t, U, μ, and β. The weight is given as

$$W = t^N \left\langle T_\tau \left[c_i(\tau_2) c_i^\dagger(\tau_1) \right] \right\rangle_{\mu+\hat{U}} \ldots \left\langle T_\tau \left[c_j(\tau_N) c_j^\dagger(\tau_{N-1}) \right] \right\rangle_{\mu+\hat{U}} (d\tau)^{N-2}, \tag{7.1.1}$$

where N is the total number of hoppings, t is the hopping parameter, and the value of the irreducible vertices is shown in Figure 5.2. Since the total weight of a path is given by integrating with respect to all internal times τ_i from 0 to β the weight includes a differential $d\tau$ for each internal time. This is nothing but a way to account for normalization of the temporal integrals. Note that the value of the first and last irreducible vertex are not accounted for in the weight because these vertices are not an intrinsic part of the bold hopping line and are instead accounted for in the general diagrammatic Monte Carlo algorithm.

Due to spatial- and temporal translation symmetry, it is sufficient to fix the starting vertex to the origin at time 0 or β. A further algorithmic simplification is to vary the external variables in the same manner as intermediate irreducible vertices. In practice, this means that G_b is sampled for all possible position- and temporal differences in the same computational run. This gives two simplifications. Firstly, the propagator is sampled according to its importance, meaning the computing time for propagation over a large distance $\mathbf{x} - \mathbf{x}'$ scales naturally with its importance $\pi(x)$, and the most important short propagation lines are sampled more thoroughly. Secondly, the normalization procedure simplifies, as a common normalization bin can be used for all external variables.

A minimal set of updates providing ergodicity consists of the updates governing the geometrical form of the path, *extend path*, and *shorten path*. These are shown in Figure 7.1. In addition, it is natural to include a *change time* update, to traverse the space of imaginary time variables.

Updates

The pair of updates governing the geometrical form of the path is shown in Figure 7.1. The *extend path* update acts on a path of length N, adds a vertex V_{N+1} with a randomly selected time τ_2 for annihilation the operator and a τ_1 equal to the annihilation time variable to the former last vertex V_N. The position of V_{N+1} is randomly chosen from the neighboring sites of V_N, meaning the update can give rise to four geometrically distinct states. In order to determine the acceptance probability $W_a(x \to x')$ for fulfillment of the detailed balance requirement, we consider the reverse update.

The *shorten path* update similarly acts on a path of length $N > 0$ and removes the last vertex in the path and corresponding hopping. Let $Q(x \to x')$ denote the probability of choosing the *extend* update in a specific direction and adding a vertex with a specific time variable τ_{N+1}

$$Q(x \to x') = \frac{P_{\text{ext}}}{4} \frac{\mathrm{d}\tau}{\beta}, \tag{7.1.2}$$

where P_{ext} denotes the probability of choosing the *extend path* type of update. The reverse update has a simpler proposal probability because the proposal state is uniquely determined from the current state.

$$Q(x' \to x) = P_{\text{short}}, \tag{7.1.3}$$

where P_{short} denotes the probability of choosing the *shorten path* type of update. Considering the relative weight $\pi(x')/\pi(x)$ where $\pi(x)$ is the weight of the a current state and $\pi(x')$ is the weight of the extended state, Eq. (7.1.1) gives

$$\frac{\pi(x')}{\pi(x)} = t \left\langle T_\tau(c_i(\tau_N)c_i^\dagger(\tau_{N-1})\right\rangle_{\mu+\hat{U}} \mathrm{d}\tau. \tag{7.1.4}$$

In conclusion, the acceptance probability of the *extend* update is given by

$$W_a = \min\left(1, \frac{\pi(x')Q(x'\to x)}{\pi(x)Q(x\to x')}\right) = \min\left(1, \frac{4t\beta \left\langle T_\tau(c_i(\tau_N)c_i^\dagger(\tau_{N-1})\right\rangle_{\mu+\hat{U}} P_{\text{short}}}{P_{\text{ext}}}\right). \tag{7.1.5}$$

Note how the time step $\mathrm{d}\tau$ cancels, ensuring that the acceptance ratio does not vanish in the continuous limit. This is an important point, as the vanishing acceptance ratios, would make the autocorrelation time diverge. The acceptance probability of the *shorten* update is given in terms of the inverse of Eq. (7.1.5).

The *extend*/*shorten* pair of updates is sufficient to obtain all possible path topologies. Due to the stochastic nature of the extend update, these updates provide ergodicity in the internal time domain as well. However, it is natural to add an update *change time* in order to reduce the autocorrelation time.

The *change time* update takes a path of length N, picks a hopping with associated time τ_i randomly and suggests to change $\tau_i \to \tau_j$ where τ_j is picked from a uniform probability distribution from the interval $[0, \beta]$. The time dependence for the irreducible vertex shown in figure 5.2 indicates that importance sampling methods [28] could increase the acceptance probability considerably for both the *extend* and *change time*. This can be seen as the value of the two-legged irreducible vertices is close to zero on a considerable part of the domain. Since the *change time* update is its own reverse, the proposal probability takes the simple form

$$Q(x\to x') = Q(x'\to x) = \frac{d\tau}{N\beta} P_{\text{change}}, \tag{7.1.6}$$

where N is the number of imaginary time variables and P_{change} is the proposal probability of the *change time* update. The change in weight originates from the change of the two neighboring irreducible vertices connected by the chosen hopping. This leaves the acceptance probability W_a to

$$W_a = \min\left(1, \frac{\pi(x')}{\pi(x)}\right) = \min\left(1, \frac{\left\langle T_\tau(c_i(\tau_i')c_i^\dagger(\tau_{i-1})\right\rangle_{\mu+\hat{U}} \left\langle T_\tau(c_j(\tau_{i+1})c_j^\dagger(\tau_i')\right\rangle_{\mu+\hat{U}}}{\left\langle T_\tau(c_i(\tau_i)c_i^\dagger(\tau_{i-1})\right\rangle_{\mu+\hat{U}} \left\langle T_\tau(c_j(\tau_{i+1})c_j^\dagger(\tau_i)\right\rangle_{\mu+\hat{U}}}\right). \tag{7.1.7}$$

τ_i' denotes the proposed time, while τ_i denotes the current time of the hopping.

In the special case where the time of the first or last hopping is changed, the starting vertex or end vertex do not affect the weight, but rather the external variables governing the sampled bold propagator $G_b(\mathbf{x}_i - \mathbf{x}_j; \tau - \tau')$.

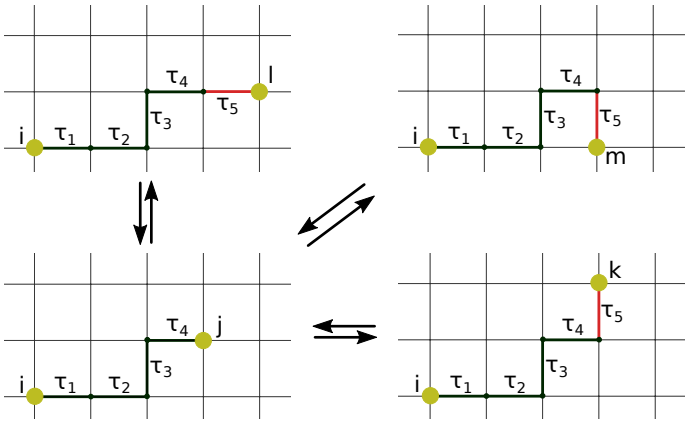

Figure 7.1: A typical path of length $N = 4$. The extend update may extend the path to any of the three possible sites k, l, or m. Although not shown, extending the path backward is also possible, giving a total of four directions. The weight is independent of the direction of the extension but is reduced due to the new irreducible vertex, time dependence, and hopping parameter. Note that the number of internal time variables increases as the path is extended.

Due to the fermionic nature of the propagators, the sign of each contribution must be accounted for. It is discussed in section 5.2.1 and is a result of the number of propagators backward in time and the number of total hoppings. This is an inexpensive calculation and may be performed before each measurement made.

A path of zero length assigned a weight of unity is added to the configuration space to normalize the resulting propagator. As this does not represent any hopping line, it is considered an unphysical state, and it does not contribute as a part of the sampled statistics.

7.2 Semi-analytical approach to boldification

The current approach, diagrammatic Monte Carlo, for the boldification process, gives a simple introduction to the method and includes simple updates and tractable convergence properties. However, the problem can be solved much more efficiently by calculating the number of possible paths analytically. This reduces the problem to only considering multidimensional integrals in time, while the number of paths is found by counting.

Given two sites i and j we calcuate the number of paths of length L connecting the sites. The number is denoted $M(L)$. Knowing $M(L)$ reduces the problem to calculating the integrals in Eq. (5.1.1) for each L up to an appropriate cutoff value $L_{\max}$. Conventional Monte Carlo integration is a suitable approach for the multidimensional

integrals.

Let the two points on lattice be $i = (0, 0)$ and $j = (r, u)$, meaning r and u denote the number of net steps required in the x- and y-direction, respectively. In order to find the number of paths M of length L, connecting the sites, we split the calculation into three cases.

Case 1: $L < |r| + |u|$

In this case, the length of the path is too short to connect the two points, giving $M(L) = 0$.

Case 2: $L = |r| + |u|$

The paths have to be monotonic in order to connect the sites. These are the shortest possible paths. The total number of paths of this length is given by $M(L) = \binom{L}{r}$. The red line in Figure 5.1 is an example of such a monotonic path.

Case 3: $L > |r| + |u|$

In this case, the length L is longer than what is minimally required. This gives rise to paths such as the green and blue path shown in Figure 5.1. We realize that for each extra step, compared to a minimal monotonic path, the path must take a step in the opposite direction. We define

$$|r| + |u| + 2x = L, \tag{7.2.1}$$

such that $2x$ denotes the number of extra steps. We split $2x$ into extra pairs of steps along the x-axis P_x and y-axis P_y such that $P_x + P_y = x$. P_x must take an integer value from on the interval $[0, x]$, which gives $x + 1$ possibilities. Without loss of generality, we assume $r > 0$ and $u > 0$ and conclude that the type of steps from site i to j must be of the following form

- Number of right steps: $(r + P_x)$
- Number of left steps: (P_x)
- Number of up steps: $(u + x - P_x)$
- Number of down steps: $(x - P_x)$

Given these possible configurations, we need to count all possible orderings of the steps. This is done by the permutations of the numbers given in the list. The total number of paths of length L is then given by

$$M(L) = \sum_{P_x=0}^{x} \binom{L}{r + P_x} \binom{L - (r + P_x)}{P_x} \binom{L - (r + 2P_x)}{u + x - P_x}. \tag{7.2.2}$$

Introducing the dummy variable $k = P_x$ and fix $x = \frac{L-r-u}{2}$ we get the slightly more general form

$$M(L) = \sum_{k=0}^{\frac{L-r-u}{2}} \binom{L}{r+k} \binom{L-(r+k)}{k} \binom{L-(r+2k)}{\frac{L+u-r}{2}-k}. \tag{7.2.3}$$

7.3 Diagrammatic Monte Carlo for full diagrammatic expansion

We have introduced methods for obtaining the value of irreducible vertices and bold hopping lines. With this, the stage is set to develop a full diagrammatic approach for the Hubbard model in the strong-coupling limit based on the irreducible vertex expansion. In the following, we describe the general framework for the diagrammatic Monte Carlo algorithm. The specific updates are described, whereas, for each update, the parity of the update must be considered. Along with the updates, we present the probabilities and weights concerning the Metropolis choice.

For algorithmic simplicity, the diagrams are represented in closed form. A diagram is considered in closed form if all bold hopping lines start and close on an irreducible vertex. This simplifies the updates because all lines can be treated equivalently. All closed-form diagrams up to order $N = 4$ in the bold hopping lines are shown in Figure 7.2. The transition from a closed diagram to an open diagram is performed through the notion of a measuring line which we define in the following.

The weight of a contribution is, according to Eq. (6.3.1), the absolute value of the kernel $|\mathcal{D}(\mathbf{x}_i - \mathbf{x}_j; \tau - \tau')|$. The kernel is given by the product of all bold propagators and irreducible vertices

$$W_{\text{tot}} = \left| \prod_n G(\mathbf{x}_{i_n} - \mathbf{x}_{j_n}; \tau_{i_n} - \tau_{j_n}) \prod_m V[\bar{O}_m] \right|, \tag{7.3.1}$$

where n runs over all bold hopping lines, except the measuring line, with their respective variables $\mathbf{x}_{i_n} - \mathbf{x}_{j_n}$ and $\tau_{i_n} - \tau_{j_n}$. m runs over all irreducible vertices $V[\bar{O}_m]$ where $\bar{O}_m$ denotes the external operators defining the irreducible vertex. As in conventional diagMC, the weight is positive, while the sign of the contribution $s = \pm 1$ is what contributes to accumulated statistics.

Measuring an observable

In order to sample an observable, more specifically the single-particle Green's function, we interpret one of the hopping lines as a *measuring line*. The measuring line is given a weight of unity, as it does not represent a physical hopping process. Note, however, that it does contribute to the weight of its corresponding irreducible vertices. When a measurement is performed, the closed diagram is interpreted as an open diagram by using the assigned measurement line.

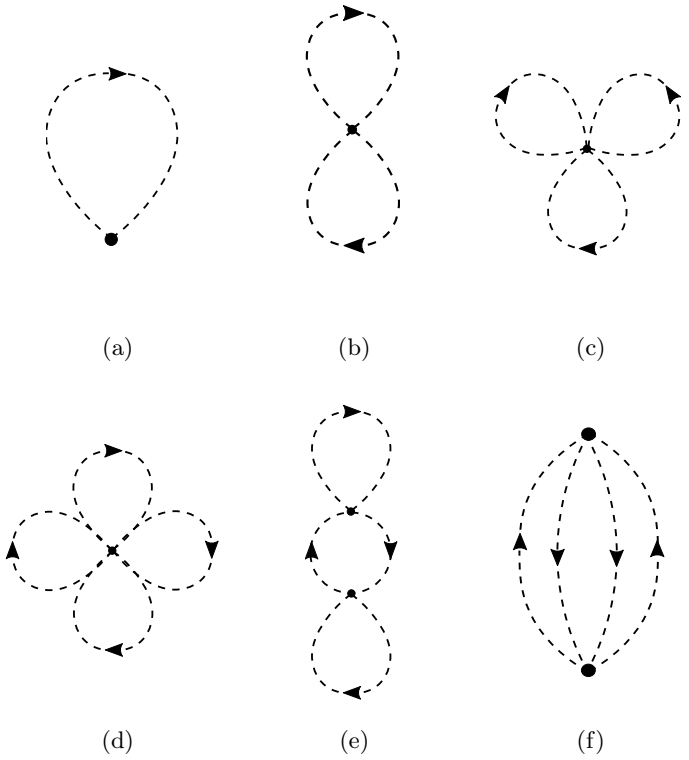

Figure 7.2: All closed diagram topologies up to order $N = 4$ in boldified hopping lines.

An important update for sampling all relevant diagram topologies is to *swap* measuring line. The *swap* update picks a bold hopping line randomly and swaps the measurement line status from the current to this line. The value of the chosen line is set to unity, and the former measuring line takes the value associated with a bold hopping line with its corresponding internal variables. A closed diagram topology may correspond to several open diagram topologies, as shown in Figure 7.3.

Data structures

In order to store a diagram as a numerical object, we introduce the following classes.

Bold hopping line A bold hopping line is stored as an object, including a set of coordinates consisting of the start time, end time, start position, end position, and a spin variable forming the set $(\tau_1, \tau_2, \mathbf{x}_1, \mathbf{x}_2, \sigma)$. Using the parameter differences $\tau_2 - \tau_1$ and $\mathbf{x}_2 - \mathbf{x}_1$, the value can be determined from the distribution $G_b(\tau_2 - \tau_1; \mathbf{x}_2 - \mathbf{x}_1)$ constructed from the boldification scheme. The value is stored as a floating-point number along with a sign. The line also carries a spin variable, which does not affect the value of the line. Further, the class has a boolean variable describing if it is the measuring line. The line

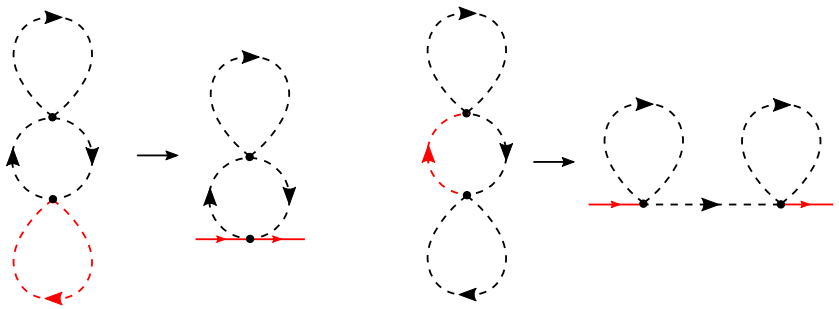

(a) (b)

Figure 7.3: Closed diagram with corresponding open diagrams with respect to the measuring line in red. One closed topology can correspond to multiple open topologies depending on the chosen measuring line.

has pointers to its originating and terminating irreducible vertices.

Irreducible vertex The irreducible vertex class consists of a list of pointers to incoming hopping lines and a list of pointers to outgoing hopping lines. The position on the lattice is stored as a pair of integers. One vertex should carry a fixed position to avoid double-counting when exploiting the spatial translation symmetry. The set of external operators, originating from the bold hopping lines with respective time dependence, uniquely determines the irreducible vertex value.

Although the value of the irreducible vertex is stored in a database, the evaluation is a relatively expensive operation. The operators originating from the bold hopping lines are in the c-basis. In order to use the convenient time dependence, the string of operators must be converted to the time trivial basis from Eq. (4.2.1). Furthermore, each possible product is obtained from the database, making the computational cost of the irreducible vertex evaluation exponentially expensive in the number of legs.

Diagram The diagram class stores all irreducible vertices and bold hopping lines. In addition, a pointer to the measuring line is stored, along with the total sign of the diagram.

7.3.1 Updates governing topology of closed diagrams

The diagrammatic expansion gives rise to a number of diagrams scaling factorial with the diagram order, and in order to traverse this space of topologies, a set of updates is needed. There are numerous possible ways to choose such updates, as long as they satisfy the ergodicity requirement; however, the proposed set has some advantages. The set is small, containing only three pair of updates, which will be presented in the following. Each update is local, meaning any evaluation for the Metropolis criterion has a constant computational cost, with respect to the size of the diagram. In contrast to other diagMC methods such as the worm algorithm [38, 39], this set of updates only allows a small fraction of unphysical diagrams, including the normalization bin and single-particle re-

ducible diagrams. A caveat is that checking for connectivity is a non-local process, and scale with the system size. Such a check is nevertheless computationally cheap for the diagrams of interest, as they are represented by relatively small graphs. For all pairs of updates we present the proposal probabilities $Q(x \to x')$, corresponding weights $\pi(x)$ and $\pi(x')$ along with acceptance probability $W_a(x \to x')$ determined from the Metropolis choice introduced in section 6.2.

Addition and removal of loops

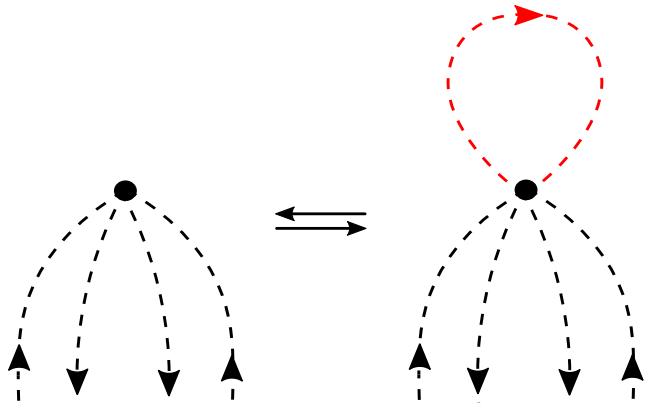

Figure 7.4: The add/remove loop update for a chosen irreducible vertex.

The *add loop/remove loop* update pair regards hopping lines starting and ending at the same irreducible vertex. It is shown in Figure 7.4. From here on, we denote such a hopping line as a loop. The *add loop* update selects a vertex randomly and proposes a loop, including a starting time, end time and a spin, (τ_1, τ_2, σ). The update increases the number of external legs for the chosen irreducible vertices by two. If the update creates an irreducible vertex with more than the maximum number of external legs, the update is automatically rejected. The size of the irreducible vertex database determines the maximum number of external legs allowed.

The *remove loop* update picks a random loop and removes it. This update is automatically rejected if the chosen loop is the measuring line. If the vertex is reduced to a two-legged vertex, it should not contribute to a physical diagram, as it is already accounted for by the boldification of hopping lines. This also leads to the update being automatically rejected. An exception is made for the case of the first order diagram, shown in Figure 7.2 a).

The Metropolis criterion for the pair of updates is found by considering the proposal probabilities and relative weights. Now let x and x' denote the state before and after a loop is added. The proposal probability of the *add loop* update is given as

$$Q(x \to x') = \frac{d\tau^2 P_{\text{add}}}{2n_v\beta^2}, \tag{7.3.2}$$

where n_v denotes the number of irreducible vertices in the diagram, 2 counts the spin possibilities and P_{add} is the probability the for which the type of update is suggested, among all possible updates.

For the reverse update, the loop to be removed is chosen independently of the number of vertices, and the proposal probability is

$$Q(x' \to x) = \frac{P_{\text{remove}}}{n_l}, \tag{7.3.3}$$

where P_{remove} denotes the proposal probability of the update, and n_l denotes the number of loops in the current diagram.

The weight of the updated diagram is affected by the additional hopping line and the change of the relevant irreducible vertex. In addition, the number of internal time variables increases, hence two infinitesimals $\mathrm{d}\tau$ are accounted for. We let the starting time and end time of the introduced loop be τ and τ'. The relative weight of the updated state is then

$$\pi(x') = G_b(\tau' - \tau)V(\bar{O}')\,\mathrm{d}\tau^2. \tag{7.3.4}$$

The relative weight of the former state is

$$\pi(x) = V(\bar{O}), \tag{7.3.5}$$

where $V(\bar{O})$ denotes the irreducible vertex with its external operators $\bar{O}$ and $G_b(\tau' - \tau)$ denotes the value of the bold loop hopping line. The update requires to look up the new potential irreducible vertex and bold hopping line in their respective databases. Consequently, the acceptance probability W_a for the *add loop* update is

$$W_a = \min\left(1, \frac{n_v\beta^2 G_b(\tau' - \tau, 0)V(\bar{O}')P_{\text{remove}}}{2(n_l + 1)V(\bar{O})P_{\text{add}}}\right). \tag{7.3.6}$$

By reversing the expression, the acceptance probability of removing a suggested loop is

$$W_a = \min\left(1, \frac{2n_l V(\bar{O})P_{\text{add}}}{n_v\beta^2 G_b(\tau' - \tau, 0)V(\bar{O}')P_{\text{remove}}}\right). \tag{7.3.7}$$

The number of loops n_l naturally changes in the transition, and this is accounted for as it changes the proposal probability. If simplicity is preferred over the optimization of acceptance rates, one can choose $P_{\text{add}} = P_{\text{remove}}$.

Addition and removal of straight lines

The *add straight lines* update selects two distinct irreducible vertices and adds two straight lines between them as shown in Figure 7.5. In this section, we denote all bold hopping lines, which are not loops, as straight lines. In order for the update to create a physical diagram with finite weight, the lines have opposite directions and carry particles of the same spin σ. Lines of this type are essential in order to give rise to non-local contributions to the single-particle propagator. Similarly to the *add loop* update, if the

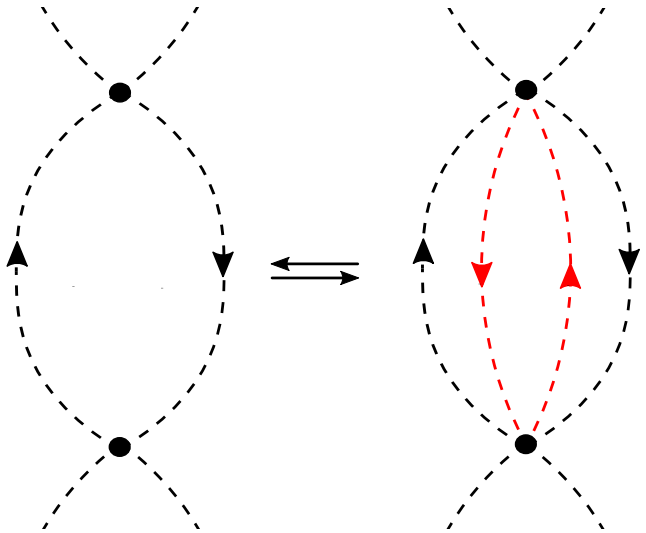

Figure 7.5: The add/remove straight lines update for two chosen irreducible vertices.

number of legs for any irreducible vertex exceeds the maximum number of legs allowed, the update is automatically rejected.

The *remove straight lines* update removes lines of the same type, given that they have the opposite direction and equal spin. Note, however, that if one of the chosen lines is the measuring line, the update is automatically rejected, as this would leave the diagram unphysical.

The *add straight lines* update is performed as follows. Given that the update is chosen with probability P'_{add}, two distinct irreducible vertices are chosen, where the order does not matter. Note that $P_{add} \neq P'_{\text{add}}$ as the first term is used for the loop update, while the primed term is for the straight line update. Parameters for the lines are suggested, including four internal time variables and a spin variable. In total, this gives a proposal probability as

$$Q(x \to x') = P'_{\text{add}} \frac{2}{n_v(n_v-1)} \frac{d\tau^4}{2\beta^4}. \tag{7.3.8}$$

Naturally, the update is rejected if the current diagram does not include more than one vertex. For the reverse update, *remove straight lines*, chosen with probability P'_{remove}, the update selects a vertex A and one of the straight lines originating at this vertex. The chosen line ends at another vertex B, as it is not a loop. A new line is chosen connecting A and B, originating at B, sharing the same spin as the first line. The proposal probability takes the form

$$Q(x' \to x) = P'_{\text{remove}} \frac{2}{n_v l_A l_{BA}}, \tag{7.3.9}$$

where l_A denotes the number of straight lines originating from vertex A and l_{BA} denotes the number of hopping lines from B to A. By interchanging A and B we get a factor 2 as this is the same update chosen in two different ways. The weight changes because of the added straight lines and affect the weight of vertex A, vertex B, in addition to the weight of the added lines. The update is computationally expensive to evaluate, but is also a proportionally large change in the topology.

The weight of the state after the addition of lines is given as

$$\pi(x') = G_b(\tau' - \tau, \mathbf{x}' - \mathbf{x})G_b(\tau'' - \tau''', \mathbf{x} - \mathbf{x}')V_A(\bar{O}')V_B(\bar{O}'')d\tau^4, \tag{7.3.10}$$

whereas in comparison, the relative value of the update is given by the previous value of the irreducible vertices is

$$\pi(x) = V_A(\bar{O})V_B(\bar{O}). \tag{7.3.11}$$

Combining the proposal probabilities and weights, the acceptance probability for adding two straight hopping lines takes the form

$$W_a = \min\left(1, \frac{P'_{\text{remove}}}{P'_{\text{add}}} \frac{(n_v - 1)}{l_A l_{BA}} \frac{2\beta^4 G_b^2 V_A(\bar{O}')V_B(\bar{O}'')}{V_A(\bar{O})V_B(\bar{O})}\right), \tag{7.3.12}$$

where G_b is shorthand notation for the added lines. The reverse update gets a reverse acceptance probability of

$$W_a = \min\left(1, \frac{P'_{\text{add}}}{P'_{\text{remove}}} \frac{l_A l_{BA}}{(n_v - 1)} \frac{V_A(\bar{O})V_B(\bar{O})}{2\beta^4 G_b^2 V_A(\bar{O}')V_B(\bar{O}'')}\right) \tag{7.3.13}$$

Addition and removal of irreducible vertex

The third pair of updates differs in nature as it changes the number of irreducible vertices and the number of bold hopping lines. Similar to the addition of straight lines, it is a relatively computationally expensive update to evaluate, with a correspondingly large change in the diagrammatic topology.

As shown in Figure 7.6, an irreducible vertex is added to an existing bold hopping line, splitting the line into two distinct lines. These new lines form the legs of the irreducible vertex with imaginary times τ_1 and τ_2 chosen randomly. In general, the update will create a diagram already accounted for through the boldification of the hopping lines. In general, unphysical states are not problematic, as long as they do not contribute to any observable and may be helpful to reduce autocorrelation. However, in the present case, allowing such diagrams in the algorithm increases the size of the configuration space a lot, without contributing correspondingly much to an efficient algorithm. A natural solution to this problem is to extend the update further to create a physical diagram. This is done by adding a loop to the introduced vertex rendering it a four-legged irreducible vertex not counted in the boldification process.

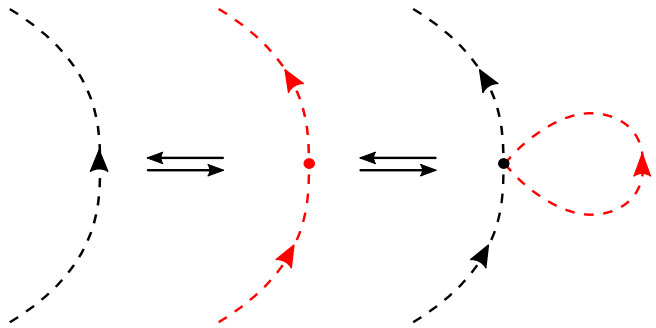

Figure 7.6: The add/remove vertex update for a chosen bold hopping line. The intermediate state is avoided by addition of a loop.

The process adds two hopping lines and a four-legged vertex in total. This includes four new internal time variables and a spin variable. As the update introduces an irreducible vertex, an internal position for the vertex must be chosen. The position should be chosen from a normalized discrete distribution similar to the underlying weight, to have a well-defined selection process. This is the idea behind importance sampling.

The simplest method is to choose a position $\mathbf{r}$ from a subset of positions around the midpoint of the neighboring vertices. The midpoint is defined as $(\bar{x}, \bar{y}) = \frac{(x_1,y_1)+(x_2,y_2)}{2}$ such that the subset takes the form

$$\{(x_i, y_i) \mid |(x_i - \bar{x})| < n \cap |(y_i - \bar{y})| < n\}, \tag{7.3.14}$$

where n is a positive integer. Assuming a decreasing correlation with distance, choosing a position from Eq. (7.3.14) would include the states with the largest weights.

In order for the *remove irreducible vertex* update to be a reverse update, it has some restrictions. The update may only delete a vertex if it is on the form shown at the rightmost end of Figure 7.6, that is, a four-legged vertex with a loop. In addition, the vertex position must be contained in a set, as defined in Eq. (7.3.14).

The update is suggested with probability P_v, and selects a hopping line randomly, with value G_b and spin σ. The spin is conserved for the two lines formed, such that the only spin variable introduced is for the hopping loop added. In total, four imaginary times are picked, and a position is uniformly chosen from the set (7.3.14). In total, this gives a proposal probability of

$$Q(x \to x') = \frac{P_v \, \mathrm{d}\tau^4}{2\beta^4 n_l V}, \tag{7.3.15}$$

where V is the number of lattice sites in the subset (7.3.14) and n_l is the total number of bold hopping lines, excluding the measuring line.

The reverse update proposal probability is given as

$$Q(x' \to x) = \frac{P_{\text{rem}}}{n_v}, \tag{7.3.16}$$

where n_v is the number of vertices in total, and P_{rem} is the probability of choosing this particular update. The proposal probability has a simple form, as any can irreducible vertex is chosen. The possibility of the update is checked subsequently. If a vertex is not fulfilling the criteria required, the update is automatically rejected. The naive proposal procedure may lead to an unnecessary amount of rejections. However, automatic rejections are computationally cheap. More sophisticated proposals are possible, but this would decrease the simplicity of the implementation.

The weight of the state x, relative to the updated state x', is given by the single line, which is cut in half.

$$\pi(x) = G_b(\text{current}) \tag{7.3.17}$$

where the argument denotes the parameters before the update $(\mathbf{x}', \mathbf{x}; \tau', \tau)$. The weight of the updated state has a richer structure, as it includes three new hopping lines $G_b(1)$, $G_b(2)$, $G_b(\text{loop})$and an additional four-legged vertex $V(\bar{O})$.

$$\pi(x') = G_b(1)G_b(2)G_b(\text{loop})V(\bar{O})\,\mathrm{d}\tau^4. \tag{7.3.18}$$

$\mathrm{d}\tau^4$ is used to normalize the four introduced temporal integrals $\int \mathrm{d}\tau$. The acceptance probability for the addition of vertex is in total given as

$$W_a = \min\left(1, \frac{2P_{\text{rem}}\beta^4 n_l G_b(1)G_b(2)G_b(\text{loop})V(\bar{O})}{n_v P_v G_b(\text{current})}\right), \tag{7.3.19}$$

while the acceptance criterion for the reverse update is

$$W_a = \min\left(1, \frac{n_v P_v G_b(\text{current})}{2P_{\text{rem}}\beta^4 n_l G_b(1)G_b(2)G_b(\text{loop})V(\bar{O})}\right). \tag{7.3.20}$$

7.3.2 Updates governing internal and external variables of diagrams

The strength of the diagrammatic Monte Carlo approach is to sample a large number of diagram topologies while performing a summation and integration over all internal variables. These are in general high dimensional sums and integrals, hence well suited for a Monte Carlo approach.

Although the set of updates presented so far is ergodic, it is natural to connect internal sets of variables without altering the topology of the diagram. This is done by introducing updates for changing internal variables as imaginary times and the position of the irreducible vertices. The update of internal variables are simple, as each update is its own inverse, $Q(x \to x') = Q(x' \to x)$. Consequently, it is unnecessary to keep track of proposal probabilities.

Change imaginary time

Changing an imaginary time variable τ is done by choosing a hopping line at random, and one of its ends, meaning either a creation- or annihilation operator. A new imaginary time

variable τ' is selected randomly from the discretized domain $[0, \beta]$. This changes both the hopping line and the associated irreducible vertex, giving the acceptance probability

$$W_a = \frac{\pi(x')}{\pi(x)} = \frac{G_b(\tau')V(\bar{O}')}{G_b(\tau)V(\bar{O})}. \tag{7.3.21}$$

Changing the time of the measuring line must be handled in a special manner, as the value of the measuring line is always unity. Consequently, the weight due to a change in external times is only affected by the change of the vertex.

Change position

In contrast to the finite imaginary time domain, the positional space is unbounded. For the *change position* update, an irreducible vertex is selected randomly. The vertex position is shifted by a single unit in either x- or y-direction. The position can be shifted in both positive and negative direction, giving a total of four possible directions. The weight of the irreducible vertex is left unchanged, as all operators are local and evaluated with respect to a local Hamiltonian. However, all hopping lines connected to the chosen vertex change weight, and must be considered for the acceptance probability. Note that even though the measuring line may change, it keeps the weight of unity. In addition, loops are naturally not affected by the change in position due to translation invariance. The acceptance probability is given by

$$W_a = \frac{\pi(x')}{\pi(x)} = \frac{\prod_i G_{b_i}(\mathbf{x}')}{\prod_i G_{b_i}(\mathbf{x})}, \tag{7.3.22}$$

where i runs over all hopping lines connected to the vertex.

7.4 Normalization of sampled distribution

The normalization bin is chosen to consist of a single unphysical diagram. It is connected to the single loop diagram shown in Figure 7.2 a) through the *add/remove loop* update. The diagram can be visualized as a vertex without any hopping lines. Note that this is the only case where removing the measuring line is not automatically rejected. The weight of the normalization diagram is set to unity. However, such a weight only has meaning relative to the weight of actual physical diagrams.

7.5 Schemes for ensuring connected and irreducible diagrams

A diagrammatic Monte Carlo approach, working directly in the thermodynamic limit, can only include connected diagrams. This is because all disconnected diagrams cancel against the partition function $\mathcal{Z}$, and is of great numerical importance as the spatial sums would lead to a configuration space $\mathcal{S}$ of unbounded total weight. The connectivity

of diagrams is a non-local property, and the computational cost typically scales with the size of the diagram.

It is sufficient to consider connectivity only after a *remove straight lines* update is accepted. This is the only update that can separate a diagram into two disconnected pieces. Evaluating the connectivity of a graph is a thoroughly discussed subject of graph theory. However, for the relatively small graphs in question, a simple breadth-first search for the two irreducible vertices related by the straight lines suffices [40]. If the update constructs a disconnected diagram, it is automatically rejected.

For each state contributing to the sampled statistics, the connectivity of the diagram is guaranteed if the previous arguments are taken into account. For obtaining a well-behaved expansion, the Dyson's equation introduced in Ref. [27] can be applied. For the state to contribute to the accumulated statistic for the so-called self-energy $\Sigma(\tau' - \tau, \mathbf{x}' - \mathbf{x})$, single-particle irreducibility is required as well. A diagram is irreducible, if it cannot be divided into two disconnected pieces, by cutting a single propagator line. Irreducibility must be considered with respect to a measuring line, as a diagram in closed form can correspond to reducible and irreducible diagrams depending on the choice of measuring line, as shown in Figure 7.3. There are numerous algorithms determining irreducibility [40]. A naive but sufficient approach for small diagrams is to find a path connecting the two external points, which is guaranteed to exist. Then connectivity is checked once more, disregarding the first path. If the diagram is doubly connected, it is irreducible and a proper contribution to the self-energy $\Sigma(\tau' - \tau, \mathbf{x}' - \mathbf{x})$.

Chapter 8

Summary and remaining steps

Following the recent work by Carlström [1], we have used perturbation theory to obtain a Feynman diagrammatic expansion for the two-dimensional Hubbard model. We make the unconventional choice of expanding in both the non-local hopping operator $\hat{t}$ and the on-site interaction $\hat{U}$. This results in a large number of possible local contractions. The local contractions are furthermore ordered into what we define as irreducible vertices. The method is reminiscent of what is done in recent developments in determinant diagrammatic Monte Carlo methods [14]. By using an operator basis with trivial time dependence, we can efficiently store the irreducible vertices in a database. It is constructed using a recursive algorithm, where each term can be calculated by considering determinants. In the calculation of irreducible vertices, the on-site interaction $\hat{U}$ is summed to infinite order, avoiding any truncation bias due to the potentially large interaction parameter U.

The irreducible vertices give rise to a diagrammatic expansion suitable for a diagrammatic Monte Carlo approach, as both the sign of the contributions and the connectivity can be handled conveniently. The distinct irreducible vertices are connected by bold propagators. The bold propagators are defined in terms of two-legged irreducible vertices and constitute the non-local contributions of the diagrams. We develop a simple diagrammatic Monte Carlo algorithm for obtaining the bold propagator distribution with a small set of updates. The algorithm serves as an introduction to a stochastic sampling of diagrammatic contributions. In addition, a semi-analytical approach is presented, where we use a closed expression for the number of directed paths connecting two lattice sites. This reduces the problem of obtaining the bold propagator distribution to solving conventional high-dimensional integrals.

The number of diagrams has a slow factorial growth in the resulting diagrammatic expansion, compared to other conventional expansions. This leaves high-order diagrams accessible. The main work of this thesis is to introduce a diagrammatic Monte Carlo implementation for this specific expansion. We use a conventional Metropolis-Hastings algorithm in the suggested implementation. A set of three pairs of updates governs the topological changes of diagrams. The updates fulfill the ergodicity requirement, making all connected diagrams in the expansion accessible. For efficiency, all updates are

local and use the provided database for irreducible vertices and bold propagators. Furthermore, the algorithm consists of updates governing the diagrams' internal variables, namely positions and imaginary times. Such updates reduce the autocorrelation time and allow efficient evaluation of internal integrals and sums. Applying the method of bold propagators in the expansion of irreducible vertices should give rise to cancellation effects alleviating the numerical sign problem.

Remaining steps

A few steps remain before a working implementation for the full diagrammatic Monte Carlo approach is in place.

The total sign of the diagrams must be stored for the general diagrammatic approach. In principle, this is determined by the odd operations introduced in section 5.2.1. However, in practice, it can be done by counting commutations for a time-ordered list of external operators for the vertices considered for each update. This procedure should be an integrated part of the local updates. It does not affect the weight of the state, and is only necessary for accepted updates.

A powerful resummation technique should be applied to improve the convergence properties of the sampled free energy $\Sigma(\omega, \mathbf{k})$. There are several possible choices, such as the Cesàro-Riesz resummation, as suggested in Ref. [33] or a Borel resummation as in Ref. [41]. In general, resummation techniques are important for obtaining sensible results for diagrammatic Monte Carlo approaches for systems suffering from the sign problem.

We suspect the algorithm to be prone to autocorrelation, compared to other recently developed diagMC approaches. An alleviation of such autocorrelation issues would be to increase acceptance rates. This can be done by applying conventional importance sampling methods to the integration over internal variables.

Bibliography

[1] J. Carlström, "Strong-coupling diagrammatics for lattice fermions and spins based on irreducible vertices," *arXiv preprint arXiv:1909.00816*, 2019.

[2] D. Kaiser, *Drawing theories apart: The dispersion of Feynman diagrams in postwar physics*. University of Chicago Press, 2009.

[3] N. Metropolis and S. Ulam, "The Monte Carlo method," *Journal of the American statistical association*, vol. 44, no. 247, pp. 335–341, 1949.

[4] J. Hubbard, "Electron correlations in narrow energy bands," *Proceedings of the Royal Society of London. Series A. Mathematical and Physical Sciences*, vol. 276, no. 1365, pp. 238–257, 1963.

[5] C. Varney, C.-R. Lee, Z. Bai, S. Chiesa, M. Jarrell, and R. Scalettar, "Quantum Monte Carlo study of the two-dimensional fermion Hubbard model," *Physical Review B*, vol. 80, no. 7, p. 075116, 2009.

[6] J. Schulte and M. C. Böhm, "Specific heat of the half-filled Hubbard chain: A Feynman path-integral Monte Carlo investigation," *Physical Review B*, vol. 53, no. 23, p. 15385, 1996.

[7] E. Loh Jr, J. Gubernatis, R. Scalettar, S. White, D. Scalapino, and R. Sugar, "Sign problem in the numerical simulation of many-electron systems," *Physical Review B*, vol. 41, no. 13, p. 9301, 1990.

[8] M. Troyer and U.-J. Wiese, "Computational complexity and fundamental limitations to fermionic quantum Monte Carlo simulations," *Physical review letters*, vol. 94, no. 17, p. 170201, 2005.

[9] P. W. Anderson, *The Theory of Superconductivity in the High-Tc Cuprate Superconductors*. Princeton University Press, 2017.

[10] N. V. Prokof'ev and B. V. Svistunov, "Polaron problem by diagrammatic quantum Monte Carlo," *Physical review letters*, vol. 81, no. 12, p. 2514, 1998.

[11] L. Landau, "On the motion of electrons in a crystal lattice," *Phys. Z. Sowjetunion*, vol. 3, p. 664, 1933.

[12] N. Prokof'ev and B. Svistunov, "Fermi-polaron problem: Diagrammatic Monte Carlo method for divergent sign-alternating series," *Physical Review B*, vol. 77, no. 2, p. 020408, 2008.

[13] N. Prokof'ev and B. Svistunov, "Bold diagrammatic Monte Carlo technique: When the sign problem is welcome," *Physical review letters*, vol. 99, no. 25, p. 250201, 2007.

[14] R. Rossi, "Determinant diagrammatic Monte Carlo algorithm in the thermodynamic limit," *Physical review letters*, vol. 119, no. 4, p. 045701, 2017.

[15] H. Tasaki, "From Nagaoka's ferromagnetism to flat-band ferromagnetism and beyond: An introduction to ferromagnetism in the Hubbard model," *Progress of theoretical physics*, vol. 99, no. 4, pp. 489–548, 1998.

[16] N. F. Mott, "The basis of the electron theory of metals, with special reference to the transition metals," *Proceedings of the Physical Society. Section A*, vol. 62, no. 7, p. 416, 1949.

[17] D. Scalapino, "Numerical studies of the 2D Hubbard model," in *Handbook of High-Temperature Superconductivity*, pp. 495–526, Springer, 2007.

[18] J. LeBlanc, A. E. Antipov, F. Becca, I. W. Bulik, G. K.-L. Chan, C.-M. Chung, Y. Deng, M. Ferrero, T. M. Henderson, C. A. Jiménez-Hoyos, *et al.*, "Solutions of the two-dimensional Hubbard model: benchmarks and results from a wide range of numerical algorithms," *Physical Review X*, vol. 5, no. 4, p. 041041, 2015.

[19] T. Matsubara, "A new approach to quantum-statistical mechanics," *Progress of theoretical physics*, vol. 14, no. 4, pp. 351–378, 1955.

[20] D. J. Griffiths and D. F. Schroeter, *Introduction to quantum mechanics*. Cambridge University Press, 2018.

[21] G. C. Wick, "Properties of Bethe-Salpeter wave functions," *Physical Review*, vol. 96, no. 4, p. 1124, 1954.

[22] M. Gell-Mann and F. Low, "Bound states in quantum field theory," *Physical Review*, vol. 84, no. 2, p. 350, 1951.

[23] G.-C. Wick, "The evaluation of the collision matrix," *Physical review*, vol. 80, no. 2, p. 268, 1950.

[24] C. M. Bender, F. Cooper, G. Guralnik, and D. H. Sharp, "Strong-coupling expansion in quantum field theory," *Physical Review D*, vol. 19, no. 6, p. 1865, 1979.

[25] P. Van Dongen, "Extended Hubbard model at weak coupling," *Physical Review B*, vol. 50, no. 19, p. 14016, 1994.

[26] L. H. Ryder, *Quantum field theory*. Cambridge university press, 1996.

[27] A. L. Fetter and J. D. Walecka, *Quantum theory of many-particle systems*. Courier Corporation, 2012.

[28] D. P. Landau and K. Binder, *A guide to Monte Carlo simulations in statistical physics*. Cambridge university press, 2014.

[29] H. Suwa and S. Todo, "Markov chain Monte Carlo method without detailed balance," *Physical review letters*, vol. 105, no. 12, p. 120603, 2010.

[30] M. Michel, S. C. Kapfer, and W. Krauth, "Generalized event-chain Monte Carlo: Constructing rejection-free global-balance algorithms from infinitesimal steps," *The Journal of chemical physics*, vol. 140, no. 5, p. 054116, 2014.

[31] W. K. Hastings, "Monte Carlo sampling methods using Markov chains and their applications," 1970.

[32] M. Peskin, *An introduction to quantum field theory*. CRC press, 2018.

[33] K. Van Houcke, E. Kozik, N. Prokof'ev, and B. Svistunov, "Diagrammatic Monte Carlo," *Physics Procedia*, vol. 6, pp. 95–105, 2010.

[34] J. Barker, "A quantum-statistical Monte Carlo method; path integrals with boundary conditions," *The Journal of Chemical Physics*, vol. 70, no. 6, pp. 2914–2918, 1979.

[35] R. Blankenbecler, D. Scalapino, and R. Sugar, "Monte Carlo calculations of coupled boson-fermion systems. I," *Physical Review D*, vol. 24, no. 8, p. 2278, 1981.

[36] J. Greitemann and L. Pollet, "Lecture notes on Diagrammatic Monte Carlo for the Fröhlich polaron," *arXiv preprint arXiv:1711.03044*, 2017.

[37] S. Kulagin, N. Prokof'ev, O. Starykh, B. Svistunov, and C. Varney, "Bold diagrammatic Monte Carlo method applied to fermionized frustrated spins," *Physical review letters*, vol. 110, no. 7, p. 070601, 2013.

[38] M. Boninsegni, N. Prokof'ev, and B. Svistunov, "Worm algorithm and diagrammatic Monte Carlo: A new approach to continuous-space path integral Monte Carlo simulations," *Physical Review E*, vol. 74, no. 3, p. 036701, 2006.

[39] J. Carlström, "Diagrammatic monte carlo procedure for the spin-charge transformed hubbard model," *Physical Review B*, vol. 97, no. 7, p. 075119, 2018.

[40] T. H. Cormen, C. E. Leiserson, R. L. Rivest, and C. Stein, *Introduction to algorithms*. MIT press, 2009.

[41] R. Rossi, T. Ohgoe, K. Van Houcke, and F. Werner, "Resummation of diagrammatic series with zero convergence radius for strongly correlated fermions," *Physical Review Letters*, vol. 121, no. 13, p. 130405, 2018.

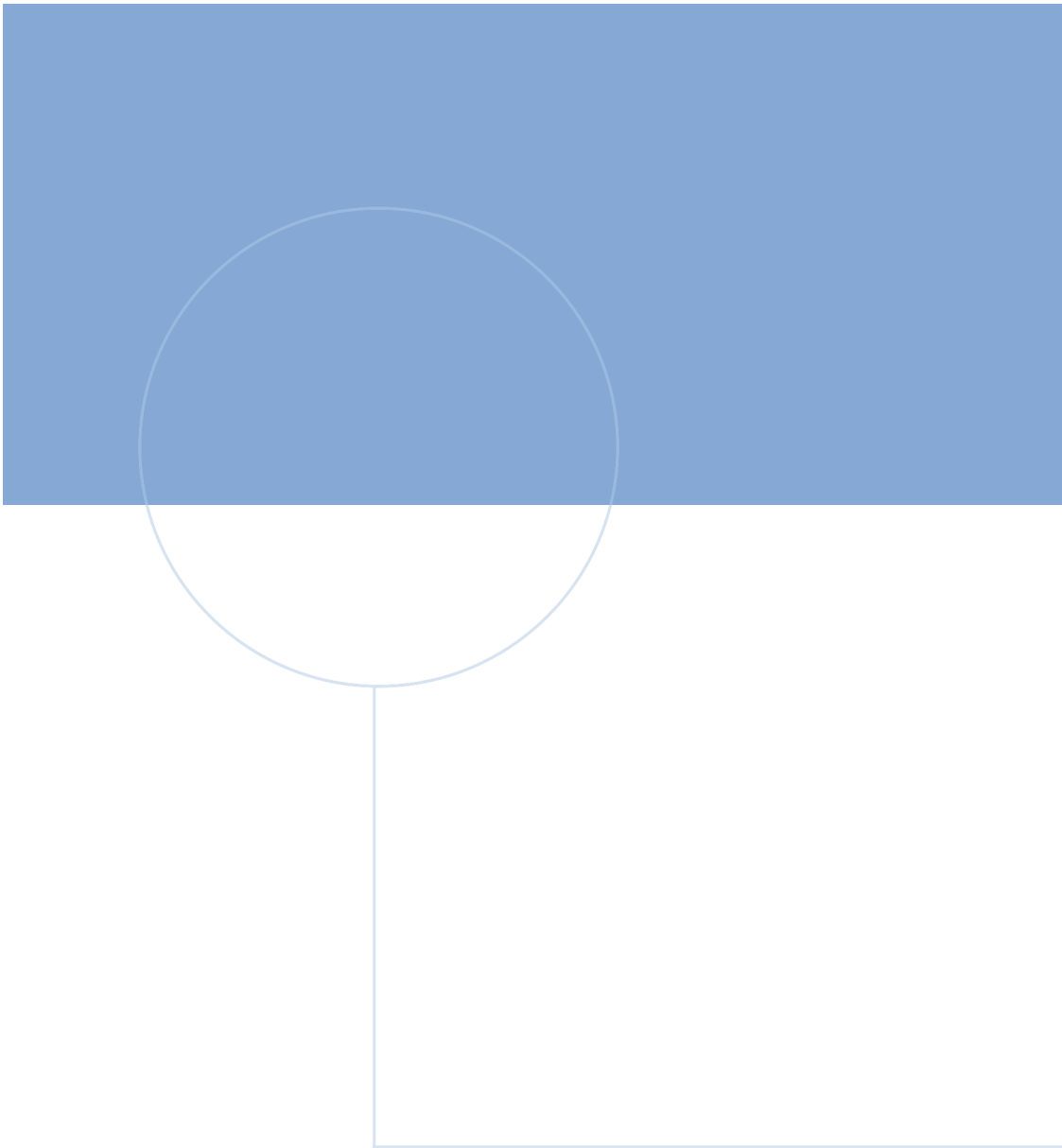

NTNU

Norwegian University of
Science and Technology